Energy Efficient Modulation Design with Unequal Error Protection for Multiresolution Image Transmission

by

Md Sabbir Hussain

Submitted in partial fulfilment of the requirements
for the degree of Master of Applied Science

at

Dalhousie University
Halifax, Nova Scotia
July 2014

To my parents

Table of Contents

List of Tables

List of Figures

Abstract

Reliable image and video communications over noisy channels has been a great challenge especially for the transmission of large volume of data over unreliable and bandwidth limited channels. One technique to deal with this problem involves taking an existing source encoder and then protecting the bits using appropriate channel coding method. However, channel coding techniques add redundant bits resulting in an increase of the required bandwidth. Also, in the case of multimedia communications, the compressed source exhibits different level of importance among different portions of the encoded bit stream which calls for Unequal Error Protection (UEP).

The unequal nature of bit importance that compressed source exhibits can be addressed by exploiting UEP within Hierarchical Quadrature Amplitude Modulation (HQAM) where different signalling points in a constellation are placed at different distances from the adjacent symbols according to their importance. This results in different bit error rates on bits these symbols represent. Conventionally, the HQAM is designed using as a basis superposition of Square Quadrature Amplitude Modulations (SQAMs) with different Euclidean distances between signalling points. However, this approach referred here to as asymmetric SQAM is not optimum in the sense of modulation power efficiency.

In this thesis, we propose first a new design for asymmetric M-ary QAM based on triangular QAM (TQAM) called asymmetric TQAM which provides considerable power gain over the asymmetric SQAM. In particular, information bits after source coding are grouped into bits according to their priority and then coded into asymmetric 64-TQAM in such a way that high priority (approximation) bits mapped onto 4-QAM have better protection from errors then the low priority (details) bits mapped onto "conventional" 16-TQAM. This is followed by bit into modulation symbol mapping to minimize Gray Mapping penalty. Then, performance analysis, in terms of power efficiency and Bit Error Rate (BER) of different UEP scenarios was carried out and presented in simulation results. Second, a scenario of image transmission is considered using the proposed asymmetric 64-TQAM. The results documenting the quality of the reconstructed images are obtained for different Signal to Noise Ratio (SNR) and the performance of the transmission system is analyzed in terms of Peak Signal to Noise Ratio (PSNR) of the received images. The results clearly show that the image transmission system using the UEP framework designed in this research outperforms the conventional and asymmetric SQAM in terms of PSNR.

List of Abbreviations Used

1D	one-dimensional
2D	two-dimensional
AWGN	additive white Gaussian noise
BER	bit error rate
BSC	binary symmetric channel
BW	bandwidth
CNR	carrier to noise ratio
DFT	discrete Fourier transform
DWT	discrete wavelet transform
IDWT	inverse discrete wavelet transform
JSCC	joint source channel coding
JPEG	joint photographic experts group
MR	multiresolution
MRA	multiresolution analysis
MSE	mean squared error
PSNR	peak signal-to-noise ratio
QAM	quadrature amplitude modulation
SER	symbol error rate
SNR	signal to noise ratio
UEP	unequal error protection
SQAM	square quadrature amplitude modulation
TQAM	triangular quadrature amplitude modulation

Chapter 1

Introduction

Communication is about trying to convey as much information as possible over a given channel with as few errors as possible. If we consider transmission of information that involves critical data, each transmitted bit is equally important. Hence, the transmission of such data requires equal error protection for all portions of the data stream. Also in some applications it is possible to guarantee the delivery of the data through the use of the Automatic Repeat Request (ARQ). However, in communication scenarios such as broadcast and multicast where reverse channel is not available, retransmission is not an option. Also in multimedia communications, the compressed source exhibits different level of importance among different portions of the encoded bitstream. This unequal nature of importance among the different sections of the encoded source information leads us to the need for unequal error protection (UEP).This means more important portions of the encoded information deserve more channel protection, while the less important portions require less channel protection [1], [2].

An inherent problem in wireless multimedia broadcasting is the sensitivity of the compressed bit-stream to data errors [3], [4], [5]. When we consider multimedia communications over wireless channels, it is necessary to protect the encoded source information with an error protection technique, where information bits are protected

according to their priority. The Discrete Wavelet Transform (DWT) used in the JPEG2000 standard is a multiresolution (MR) source coder where the source information is split into different bins in which information content ranges from coarse to fine. To pair with this multiresolution source coding it is equally important to design an adaptive channel coding framework which can offer a hierarchy of "resolution" of noise immunity in order to adapt to different need of channel protection among different portion of the encoded bit stream [6]. Such a MR modulation framework was proposed by Hiten and Ilow [7] where the well known Square Quadrature Amplitude Modulation (SQAM) was used as a modulation scheme. Although SQAM offers easy detection but is not optimum in terms of energy efficiency.

In this thesis, we design a novel multiresolution modulation, which is also referred to interchangeably in the literature as embedded, superposition or hierarchical modulation scheme [8], [9], [10]. This asymmetric 64-ary Triangular Quadrature Amplitude Modulation (TQAM) with UEP is a superposition of 4-QAM (or QPSK) and modified 'conventional" 16-TQAM with the specialized bit mapping. The proposed modulation outperforms in terms of energy efficiency the well known conventional 64-ary SQAM with equal error protection and the asymmetric 64-SQAM with UEP. When examining the benefits of the proposed asymmetric 64-TQAM in practical transmission systems, in this work, we restrict our attention to "image" as our multimedia source. For the compressed image transmissions, the sensitivity of different portions of the data stream to errors is addressed through the use of UEP, where information symbols are protected according to their importance [11]. Secondly, an image transmission scenario is carried out to and the reconstructed images are analyzed in terms of Peak Signal to Noise Ratio (PSNR). It is expected that the research results presented in this thesis will contribute to the advancement of future standards for digital video broadcasting (DVB) such as DVB-terrestrial (DVB-T), DVB-satelite (DVB-S) and DVB-handhelds (DVB-H) [12].

1.1 Source Coding

Images and videos are moved around the World Wide Web by millions of users almost in a nonstop fashion, and then, there is television (TV) transmission round the clock. The transmission of these visual media in digital form alone will require far more bandwidth than what is available for the Internet, TV, or wireless networks. Therefore, one must find ways to format the visual media data in such a way that it can be transmitted over the bandwidth-limited TV, Internet, and wireless channels in real time. This process of reducing the image and video data so that it fits into the available limited bandwidth or storage space is termed data compression. It is also called source coding in the communications field [13].

The objective of source coding in multimedia communication is to exploit the redundancy in the source such that a smaller number of bits can be used to represent the multimedia source while maintaining an acceptable visual quality for the decompressed data. For example, The redundancy of an image resides in the correlation of the neighboring pixels. In general, image coding algorithms can be classified into progressive, embedded or scalable source coders [14] and most of them employ Discrete Wavelet Transform (DWT) [15] as the transform coding technique due to its computational efficiency and compression potentials. DWT was first employed for image coding by Shapiro's embedded zero-tree wavelet coder [16] and then by Said and Pearlman for SPIHT based image coding [17] which gained significant improvements over Discrete Fourier Transform (DFT) based image coding. The latest image compression DWT-based standards like JPEG2000 [18], [19] are still evolving to achieve even higher robustness against channel errors, especially in wireless environments. DWT based image compression produces bit sub-streams with different importance levels that are matched with Unequal Error Protection (UEP) levels. In this paper, we simplify the source coding technique as conventional 2D-DWT for ease of designing our modulation scheme.

1.1.1 Wavelet Transform

Often signals we wish to process are in the time-domain, but in order to process them more easily, other information such as frequency, is required [20]. Discrete Fourier Transform (DFT) is very useful at providing frequency information that cannot be seen easily in the time domain. DFT helps analyze the frequency domain characteristics of the signal within the DFT time (or space, for images) window. IT is based on sinusoids and can capture only frequencies in the steady state, that is, such a transform can enumerate the different frequencies present in the signal being analyzed from start to finish but cannot capture the moments that such frequencies begin or end. In the same manner, transforms based on sinusoids cannot pinpoint locations where activities occur in an image. In other words, DFT cannot identify the occurrence of the various frequency components at different moments in time (or locations in space). With DFT, time-frequency (or space-frequency) localization of a signal is not possible for signals whose characteristics change with time (or space), known as non-stationary signals [13], [15], [21].

On the other hand, in wavelet transform, frequency components of a signal are analyzed using different resolutions of the basis functions. Rather than examining entire signals through the same window, different parts of the wave are viewed through different size windows (or resolutions). High frequency parts of the signal use a small window to give good time resolution, low frequency parts use a big window to get good frequency information. Figure 1.1 shows different transforms provided different resolutions of time and frequency. When compressing an image, if we can distinguish areas of intense activity from flat regions, we may be able to allocate different number of bits of quantization to these different regions, thereby achieving a high compression without sacrificing visual quality. Even though this is possible with transforms based on sinusoids, wavelets are more efficient because of their inherent property of capturing transients. The key aspect of the wavelet transforms is that different frequency components of a signal are analyzed using different resolutions of

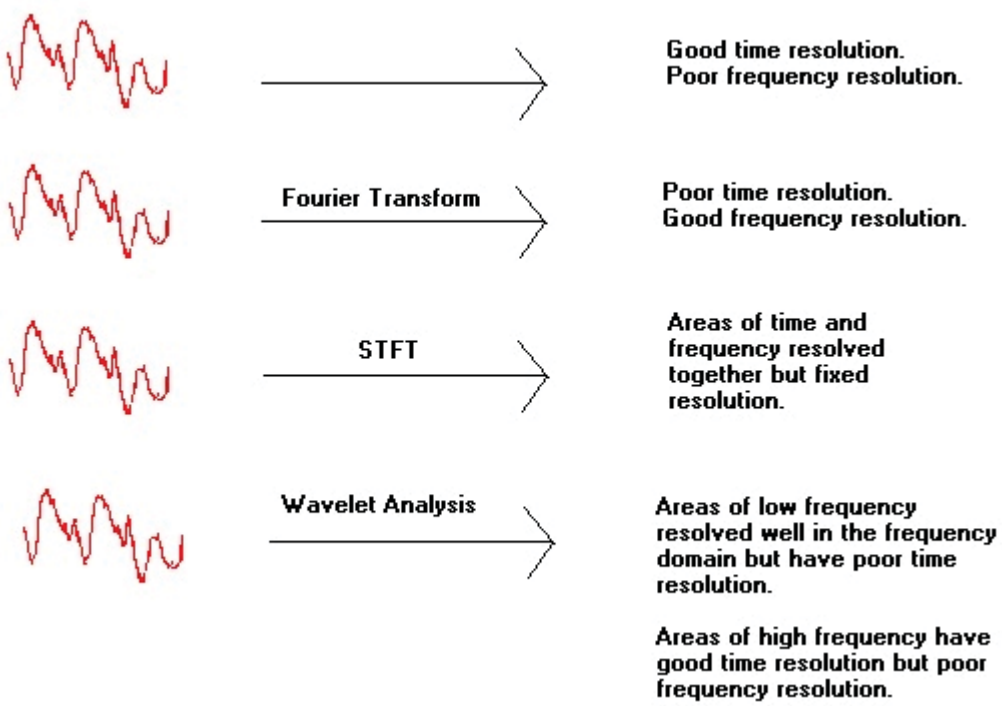

Figure 1.1: The different transforms provided different resolutions of time and frequency.

the basis functions. In other words, the signal is coded (or analyzed) using different scaled and translated versions of the basis functions.

Wavelet transform is an efficient tool for analyzing non-stationary signals. It has been extensively used in various areas of science and engineering, especially in image processing.

1.1.2 Discrete Wavelet Transform

The discrete wavelet transform (DWT) is a linear transformation that generally operates on a data vector having length of an integer power of two, transforming into a numerically different vector of the same length. DWT separates data into different frequency components and studies each component with resolution matched to it's scale. For numerical computation, scales s and translations τ must be discrete. Since,

scales of power two is adopted and all wavelets in a family must be equally involved to code a signal, translations and scalings must be adjusted accordingly. This is done by the following relations.

$$s = 2^{-j} \tag{1.1}$$

$$\tau = k2^{-j} = ks \tag{1.2}$$

where j and k are integers.

Using the relations in (1.1) and (1.2), we can write the wavelet function as

$$\psi\left(\frac{t-\tau}{s}\right) = \psi\left(\frac{t-ks}{s}\right) = \psi\left(2^j t - k\right) \tag{1.3}$$

To generalize the wavelet function for a wavelet family, a scaling factor of $2^{j/2}$ must be applied to this equation. Thus scaled and translated version of the mother wavelet $\psi(t)$ becomes

$$\psi_{jk}(t) = 2^{j/2}\psi(2^j t - k) \tag{1.4}$$

where j and k indexes the scale and shift respectively. Similarly all scalings and translations of the father wavelet $\varphi(t)$ can be written as

$$\varphi_{jk}(t) = 2^{j/2}\varphi(2^j t - k) \tag{1.5}$$

1.1.3 Multiresolution Analysis

While scaling functions are adequate to code a signal, it is more efficient to code a signal using both scaling and wavelet functions together. A wavelet function can be derived from the father wavelet.

For a function $f(t)$ to be coded in terms of the scaling functions $\varphi_{jk}(t)$ alone implies that the expression

$$f(t) \approx f_j(t) = \sum_{k=-\infty}^{\infty} c_j[k]\varphi_{jk}(t) = \sum_{k=-\infty}^{\infty} c_j[k]2^{j/2}\varphi(2^j t - k) \tag{1.6}$$

must hold for some set of coefficients $c_j[k]$ and some scale $s = 2^{-j}$. The index j must be large enough so that a scale 2^{-j} is small enough to capture all the signal details.

The scale j belongs to a subspace S_j and the set of functions $f_j(t)$ can be perfectly described by the scaling functions.

While scaling functions can gain a certain degree of accuracy, efficiency can also be gained by using wavelet functions as well. For the wavelet function we can define a subspace W_j that complements the subspace S_j to describe the function f_{j+1} in subspace S_{j+1}. This can be expressed as follows

$$\begin{aligned} f(t) \approx f_{j+1}(t) &= \sum_{k=-\infty}^{\infty} c_{j+1}[k]\varphi_{(j+1)k}(t) = \sum_{k=-\infty}^{\infty} c_j[k]\varphi_{jk}(t) + \sum_{k=-\infty}^{\infty} d_{j+1}[k]\psi_{jk}(t) \\ &= \sum_{k=-\infty}^{\infty} c_j[k]2^{j/2}\varphi(2^j t - k) + \sum_{k=-\infty}^{\infty} d_j[k]2^{j/2}\psi(2^j t - k) \end{aligned} \tag{1.7}$$

Thus, the subspace S_j represents the coarser approximation of the signal $f(t)$ and subspace $S_j + 1$, represents the finer approximation of $f(t)$. Thus the subspace W_j plays the role of adding details to S_j for a better approximation of $f(t)$. This idea of different levels of multiresolutions can be illustrated by the following expressions.

$$\begin{aligned} S_3 &= S_2 \cup W_2 \\ &= (S_1 \cup W_1) \cup W_2 \\ &= ((S_0 \cup W_0) \cup W_1) \cup W_2 \\ &= S_0 \cup W_0 \cup W_1 \cup W_2 \end{aligned} \tag{1.8}$$

An important property of every scaling function $\varphi(t)$ is that it can be built from translations of half-scaled copies of itself, $\varphi(2t)$, according to the general equation

$$\varphi(t) = \sum_{k=-\infty}^{\infty} \sqrt{2} h_0[k]\varphi(2t - k) \tag{1.9}$$

where $h_0[k]$ are called the scaling function coefficients and $\sqrt{2}$ is a scaling factor that keeps the energy of scaling functions at every scale the same. Equation (1.9) is called a multiresolution analysis (MRA) equation.

1.1.4 Two Dimensional Discrete Wavelet Transform

The **analysis equation** which implements the DWT, are:

$$c_j[k] = \sum_{m=-\infty}^{\infty} c_{j+1}[m]h_0[m-2k] \tag{1.10}$$

$$d_j[k] = \sum_{m=-\infty}^{\infty} c_{j+1}[m]h_1[m-2k] \tag{1.11}$$

These equations relate the DWT coefficients at a finer scale, $j+1$, to the DWT coefficients at a coarser scale, j. Figure 1.2 illustrates the process of one-dimensional DWT decomposition The **synthesis equation**, which implements the Inverse DWT

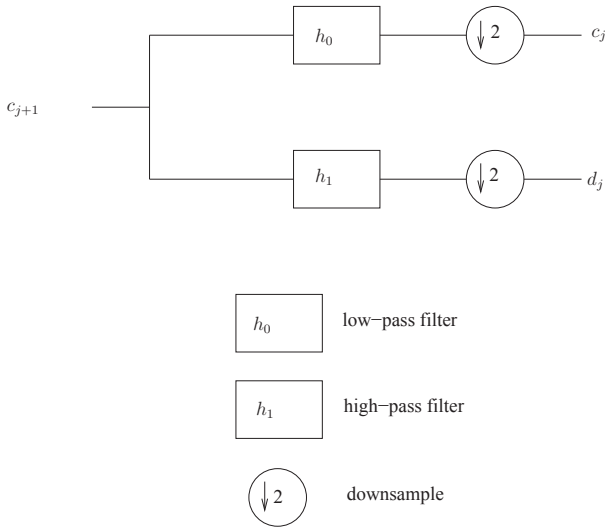

Figure 1.2: One-dimensional signal decomposition

(IDWT), is:

$$c_{j+1}[k] = \sum_{m=-\infty}^{\infty} c_j[m]h_0[k-2m] + \sum_{m=-\infty}^{\infty} d_j[m]h_1[k-2m] \tag{1.12}$$

However, images are two-dimensional signals requiring two-dimensional wavelet treatment. Thus we need two dimensional discrete wavelet transform (2D-DWT) for image compression and this is done using the concept of filter banks. Filters of different cut-off frequencies analyze the signal at different scales. Resolution is

changed by the filtering, the scale is changed by up-sampling and down-sampling. If a signal is put through a high and low pass filter, a high pass filter will keep high frequency component and suppress low frequency component. On the other hand, a low pass filter will keep low frequency component and suppress high frequency component. then the signal is effectively decomposed into two parts, a detailed part (high frequency), and an approximation part (low frequency). The subsignal produced from the low filter will have a highest frequency equal to half that of the original. The resolution has also been changed, the filtering made the frequency resolution better, but reduced the time resolution. The approximation subsignal can then be put through a filter bank, and this is repeated until the required level of decomposition has been reached. The ideas are shown in figure 1.3

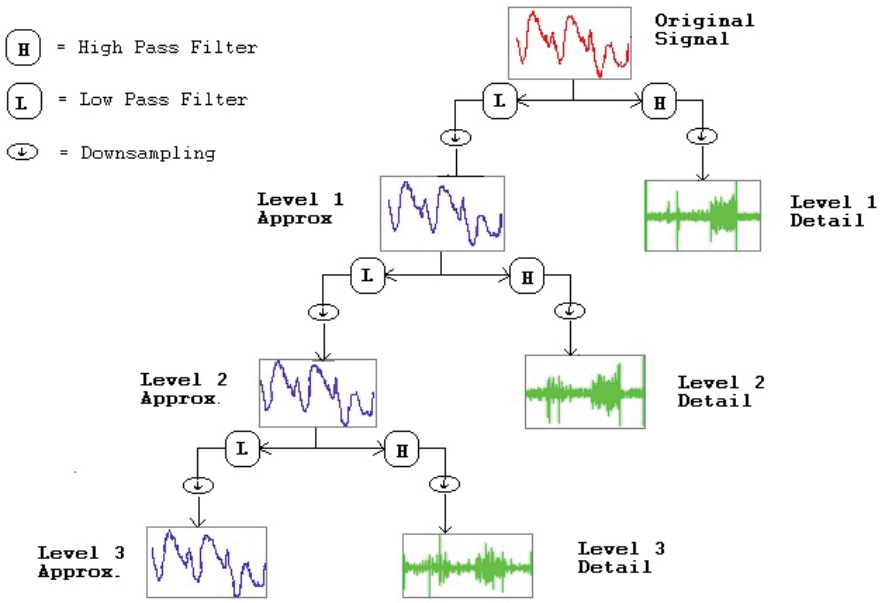

Figure 1.3: Wavelet decomposition using filter banks

2D-DWT is accomplished using 1D-DWT across rows and columns of an image in succession. Figure 1.4 shows single level DWT decomposition of the original image of size $N \times N$ into transform coefficients divided in four portions, called **subbands**, of equal size $(\frac{N}{2} \times \frac{N}{2})$. The parts LL, LH, HL and HH, referred to as layers, are

obtained from separate applications of a low-pass filter and a high-pass filter. The subband LL comprises of the coarse information of the wavelet coefficients and are formed after low pass filtering along both the row and columns. Other three subbands LH, HL and HH refers to the horizontal, vertical and diagonal details respectively and represent the finer scale of the wavelet coefficients. In literature, these subbands are juxtaposed in a particular order, as shown in the Figures 1.4b and 1.4c, for a descriptive view of the decomposed image consisting of $N \times N$ coefficients consistent in dimensionality and cardinality with the original image of $N \times N$ pixels.

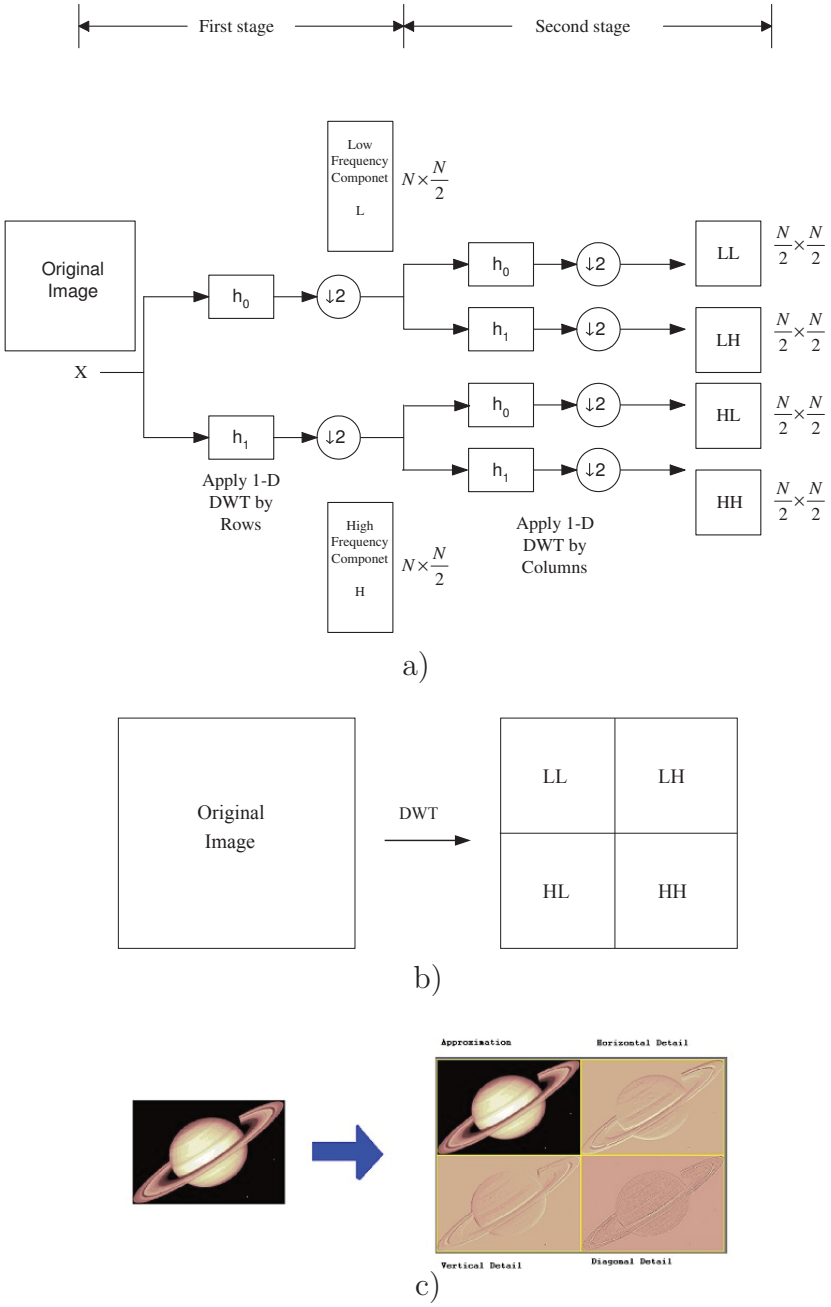

Figure 1.4: a) Two-dimensional DWT for image decomposition b) Juxtaposition of subbands for descriptive representation of DWT c) First level 2D-DWT Saturn image decomposition.

1.1.5 Performance Metrics

The performance metrics used to measure the quality of the image reconstructed from the received and decoded bitstream are mean squared error (MSE) and **peak signal to noise ratio** (**PSNR**). Assuming that a black and white image contains $M \times N$ pixels, where the pixel values range between black (0) and white (255), these metrics are defined as follows [22]:

1. MSE

$$MSE = \frac{1}{M} \cdot \frac{1}{N} \cdot \sum_{i=1}^{M} \sum_{j=1}^{N} [f(i,j) - f'(i,j)]^2 \tag{1.13}$$

where $f(i,j)$ represents the pixel value of the original image and $f'(i,j)$ represents the pixel value of the reconstructed image.

2. PSNR

$$PSNR = 10 \log \left(\frac{255^2}{MSE} \right) \tag{1.14}$$

1.2 Joint Source-Channel Coding

Source coding is a data compression process that aims at removing as much as possible redundancy from the source signal, while channel coding is the process of intelligent redundancy insertion which creates some kind of protection from the channel noise [23]. In the majority of the communications system design algorithms, the basic design procedure consists of selecting a source encoder which changes the source sequence into series of equally likely binary digits followed by a channel encoder which accepts the binary digits and puts them into a suitable form of reliable transmission

over the channel. However, this idea of separate source and channel coding holds if the communication is point to point, this hypothesis is not realistic for broadcasting communications with multi-path fading. The reason being is, for a different source or channel we have to allow infinite complexity and delay in the coders in order to reach optimality. Evidently this is problematic for real-time communication. Also such systems tend to break down completely when the channel quality falls under a certain threshold, and the channel code is no longer capable of correcting the errors [24].

When operating under a delay-constraint on a time-varying channel, it is generally no longer optimal to regard the two coders separately and we have to jointly optimize the source coder and the channel coder and the result is some sort of joint source-channel coding (JSCC) [24]. JSCC can be achieved in a number of different ways. Zahir Azami et al. (1996) [23] gave a brief overview of the most prominent JSCC techniques like unequal error protection (UEP), index assignment (IA), co-optimized vector quantizing and IA (i.e. channel optimized vector quantizer), and direct modulation organizing schemes. However, to match our wavelet transform based multiresolution coder, we are using unequal error protection (UEP) based on multiresolution (MR) modulation for JSCC technique.

1.2.1 Unequal Error Protection

One way to maintain the performance in noisy environment is by better protecting the more sensitive information which are suspected to contribute to greater errors. This method is known as **unequal error protection** (**UEP**). One of the most efficient ways to achieve UEP is by arranging the modulation space in such a way that the coarse or high priority information is better protected from errors than fine or low priority information.

In conventional 16-ary qam showed in figure 1.5, all the signalling points are equally spaced from each other with a minimum distance d_{min}=2d. We can calculate

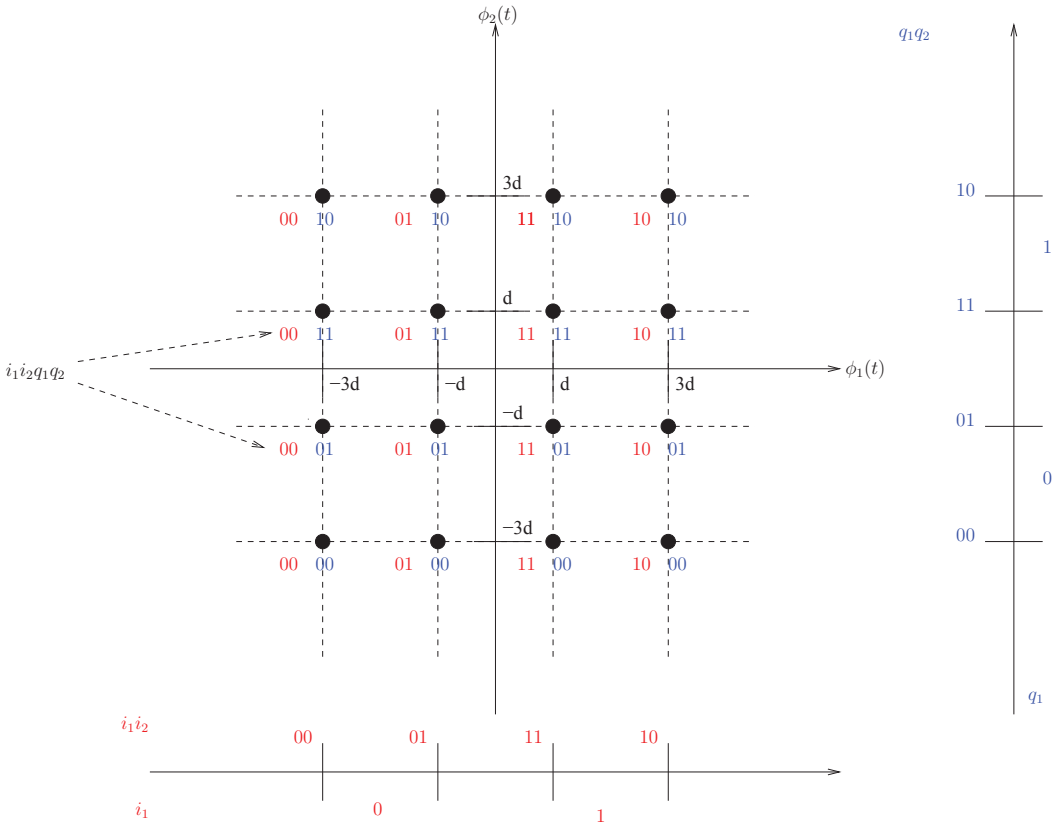

Figure 1.5: Conventional 16-ary QAM

the *symbol error rate*(Pe_{sym}) and *bit error rate*(BER) as following two equations [25]

$$Pe_{sym} \simeq \frac{M_{min}}{2} \cdot \text{erfc}\left(\sqrt{\frac{d^2_{min}}{4N_0}}\right) \tag{1.15}$$

$$BER \simeq \frac{1}{\log_2 M} Pe_{sym} \tag{1.16}$$

where N_o is the power spectral density of the noise given in *Watts/Hz*, M_{min} is the number of neighboring symbols to which we achieve minimum distance and is the highest among all signalling points. In the case of 16-ary QAM in figure 1.5, the number of neighboring symbols to which we achieve minimum distance is 4 and hence, M_{min}=4 . Although, the equation(1.16) is only correct if the bit mapping is done according to Gray encoding. Gray encoding is a bit mapping strategy where the neighboring symbols, with which we achieve M_{min}, differ in only one bit. Thus Gray

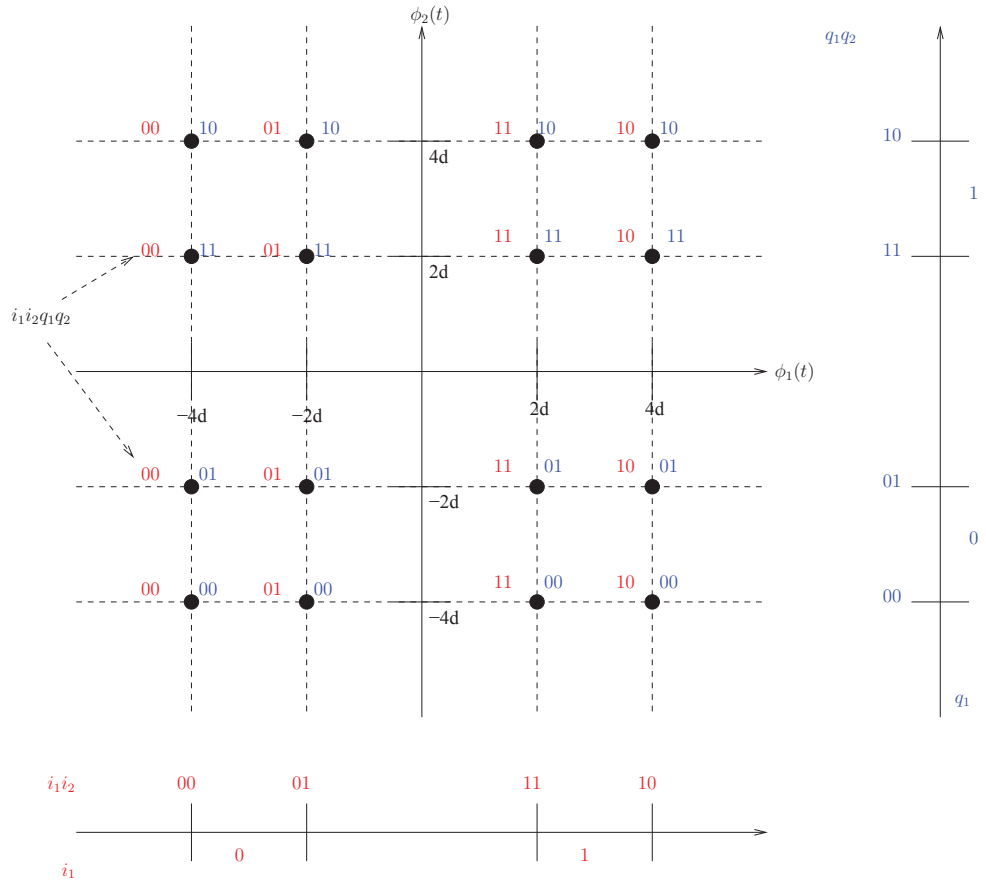

Figure 1.6: An example of asymmetric 16-ary QAM (Asymmetric 16-ary SQAM)

encoding minimizes bit errors by causing adjacent symbols to only be one bit differ from their neighbors. By using Gray encoding, the most possible case of interfering of adjacent or neighboring symbol, will result in only one bit in error. Also for practical purposes it is necessary to relate the minimum distance d_{min} with *average energy per symbol* E_s. In the case of figure 1.5 E_{sqam}^{conv}=$10d^2$. Since, d_{min} for conventional 16-QAM showed in figure 1.5 is 2d, based on equation(1.15) the equi-spaced conventional 16-ary QAM, the SER is given as,

$$Pe_{sqam}^{conv} \simeq \frac{4}{2} \cdot \text{erfc}\left(\sqrt{\frac{E_s{}^{conv}}{N_0}\frac{1}{10}}\right) \tag{1.17}$$

For ease of explanation, we will mention the equi-spaced QAM or constellation with equal error protection showed in figure 1.5 as conventional QAM and unequally-spaced

QAM or constellation with unequal error protection showed in figure 1.6 as asymmetric SQAM where SQAM stands for Square Quadrature Amplitude Modulation.

An example of UEP using 16-ary QAM is showed in figure 1.6, We can observe here that, unlike conventional 16-ary QAM in figure where each symbol is equally spaced from each other, in the asymmetric constellation showed in figure 1.6, the signalling points have co-ordinates different from the conventional scheme resulting in *unequal* inter-distances between adjacent symbols. Unlike conventional 16-QAM where we have only one minimum distance d_{min}, asymmetric 16-QAM has two minimum distances. In the case of figure 1.6, inter-cloud symbols are separated with a minimum distance d_{min1}=2d and inter-cloud symbols are separated with a distance d_{min2}=4d, and average energy per symbol is calculated as E_{sqam}^{asymm}=$20d^2$. So, we can rewrite equation(1.15) for asymmetric 16-ary SQAM as,

$$Pe_{sqam}^{asymm} \simeq \frac{4}{2} \cdot \text{erfc}\Big(\sqrt{\frac{{E_s}^{asymm}}{N_0}\frac{1}{20}}\Big) \tag{1.18}$$

However, in equation(1.19) and equation(1.18), we did not differentiate between more protected bits and assumed worst case scenario.

1.2.2 Triangular Quadrature Amplitude Modulation

Conventional and asymmetric 16-QAM showed in figure 1.5 and figure 1.6 are both based on square structure, where signalling points are placed at the vertexes of squares. Since SQAM maintains high minimum distance and has easy detection methods, it is numerously used by various digital communications system. However, despite of the easy detection method, SQAM is not optimum in terms of power efficiency. In [26] Park proposed quadrature amplitude modulation scheme based on triangular structure, which outperforms well known SQAM in terms of energy efficiency. Figure 1.7 shows a conventional 16-ary Triangular Quadrature Amplitude Modulation or conventional 16-TQAM. We can see that unlike in the SQAM where signalling points are placed at the vertexes of squares, in 16-TQAM, signalling points

are placed at the vertexes of equilateral triangles. Since this is a conventional constellation, each symbol is equally distanced from each other with minimum distance d_{min}=2d, which is as same as for conventional 16-SQAM in figure 1.5. However, unlike for conventional 16-SQAM where the average energy per symbol was calculated as $10d^2$, for conventional 16-TQAM average energy per symbol $E_{tqam}^{conv} = 9d^2$. Also, unlike conventional 16-SQAM where each symbol has 4 neighboring symbols within the minimum distance, in conventional 16-TQAM, each symbol has 6 neighboring symbols within minimum distance. So in this case, $M_{min} = 6$. So, we can rewrite equation(1.15) for asymmetric 16-ary TQAM as,

$$Pe_{tqam}^{conv} \simeq \frac{6}{2} \cdot \text{erfc}\Big(\sqrt{\frac{E_s{}^{conv}}{N_0}\frac{1}{9}}\Big) \tag{1.19}$$

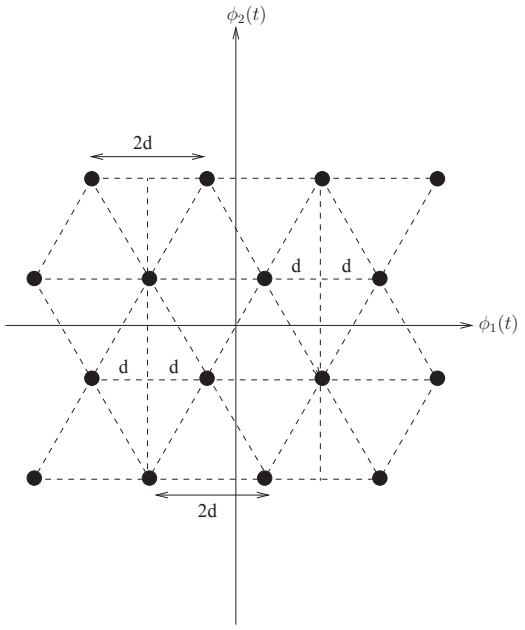

Figure 1.7: Conventional 16-ary TQAM

1.3 Research Objective

The research in this thesis has following objective towards the design of asymmetric TQAM for joint source channel coding:

1. The first objective is to design a modulation scheme for unequal error protection which outperforms the conventional scheme in terms of power gain and bit error rate. For some selective form of communications (i.e. multimedia communications), it is necessary to optimize the error protection in different portion of the source according to priority. The sole purpose of this research is to design an asymmetric modulation scheme to fit the criteria of unequal error protection based communications.

2. The second objective is the bit mapping for the asymmetric modulation scheme. According to the communications scenario, source bits are divided into HP and LP bits, where bits have different levels of vulnerability to noise. In this research we attempt to vary the Euclidean distance between symbols in the objective to analyze the performance of our designed asymmetric modulation scheme in terms of average energy per symbol and BER.

3. The third objective is to simulate an image transmission scenario for different ratios of Euclidean distances and different values of SNR using the asymmetric modulation scheme. We will observe and analyze the different degrees of distortion in the reconstructed images for different SNR, and different minimum distance ratio.

1.4 Thesis Organization

This thesis is organized into four chapters. The first chapter is the introduction and theoretical background where theoretical background of the areas important to the

research is presented, which includes topics related to both source coding and channel coding. This is followed by discussion about research objective.

In chapter 2, the technique of MR modulation framework deigned in this research is discussed. Then calculation and discussion of average energy per symbol of 64-ary SQAM and 64-ary TQAM is carried out. This is followed by bit mapping strategy and simulation results.

In chapter 3, an image transmission framework is presented using the MR modulation technique designed in this research. Then the reconstructed images are analyzed in terms of PSNR. Finally the simulation results are presented and discussed.

Finally, chapter 4 presents the conclusion and thesis contribution. Potential scopes for future research is also discussed.

Chapter 2

Design of Asymmetric Modulation Scheme for UEP

In this chapter, we develop a new design for M-ary QAM with UEP, which has better energy efficiency in comparison to conventional M-ary SQAM with UEP. Our goal is to design an asymmetric constellation for lower priority bits based on triangular structure, while using symmetric QPSK for higher priority bits. An optimal bit mapping strategy is also proposed to maintain low detection complexity.

In Section 2.1, we first explain the system model with Binary Symmetric Channel (BSC). Then the Multiresolution (MR) framework with Joint Source-Channel Coding (JSCC) is discussed.

In Section 2.2, we propose a new design for M-ary QAM based on triangular structure, and compare the average energy per symbol with conventional M-ary QAM and asymmetric M-ary QAM . For convenience, we will refer the conventional M-ary QAM as conventional SQAM, asymmetric M-ary QAM as asymmetric SQAM and asymmetric triangular QAM as asymmetric TQAM. Different scenarios for UEP for conventional and asymmetric SQAM and TQAM are analyzed by varying minimum distances between the symbols with the goal of finding new design with improved energy efficiency. This is followed by the presentation of bit mapping strategy for

asymmetric TQAM.

In Section 2.3, we show the simulation results obtained in this research. The results of simulation using different ratios of minimum distances are presented for different constellation designs of asymmetric TQAM. These results are then analyzed by comparing different BERs of different constellation designs for a fixed SNR.

2.1 Multiresolution Modulation

In this section, we will first discuss the simplified block diagram of the image transmission system using 2D-DWT as source coding technique. Then the concept of MR modulation is discussed in detail and the process of merging source coding with channel coding to obtain Joint Source-Channel Coding (JSCC) is explained.

Figure 2.1 shows a canonical block diagram employed in this research. In this model, the original image is first compressed and encoded using source encoding based on 2D-DWT and is then transmitted. One noticeable advantage of DWT is it partitions the source information into two parts: the approximation and detail. The approximation comprises the high-scale, low frequency components of the signal, and carries data which is important and more vulnerable to channel errors. The detail bits carry less important data, and are hence less important for reconstructing the image. The modulator, demodulator and AWGN channel is viewed as the binary symmetric channel (BSC). At the receiving end the decoder simply employs the reverse technique described above for reconstructing the image.

When dealing with a multimedia source such as an image, having a multiresolution architecture enables efficient adaptation to changing bit rates and bandwidth. To build an efficient end-to-end broadcast system we have to design its transmission constellation according to the source coding scheme. We have already discussed that in 2D-DWT the image is split into different bins in which information content ranges from coarse to fine. For acceptable reconstruction of the image, coarse information

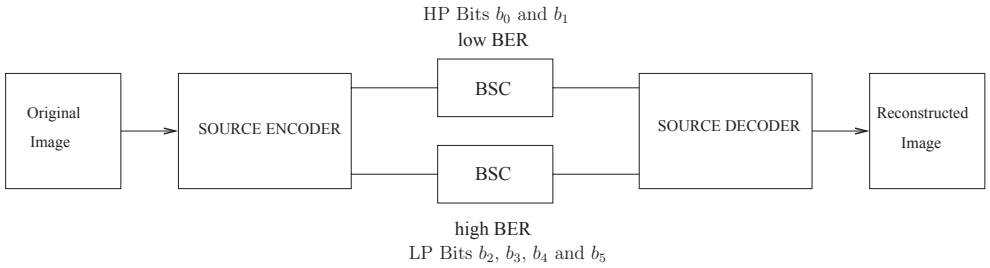

Figure 2.1: System Model

is more important than fine, and hence, has higher sensitivity to channel noise. This unequal need for error protection can be addressed by MR modulation where important parts of the compressed source can be protected better by organizing modulation space properly.

In 1998 Kozintsev and Ramchandran [27] proposed such an image transmission system using MR Modulation over a time-varying channel. Figure 2.2 shows an example of MR Modulation used in [27]. Here, each set of closed symbols constitutes a cloud, with satellites symbols surrounding it. The clouds are separated by a greater distance d_2 which conveys better noise immunity, while the satellites are separated by smaller distance d_1 and have less noise immunity. The coarse information is carried by the clouds, while inside each cloud, the mini constellations or satellites provide fine information. If parts of the coarse information are lost during transmission, the receiver will be unable to decipher which cloud was transmitted. On the other hand, the loss of detail information occur when the receiver confuses one intra-cloud signal point for another. Thus, by pairing the multiresolution source coding output from 2D-DWT with a multiresolution modulation scheme we jointly created the source coder and the channel coder and the result is a combination of Joint Source-Channel Coding (JSCC).

The transmitter section is shown in figure 2.3. The source encoder apportions compressed bit streams of the image into approximation and detail bit stream. In our work, we only consider approximation bits for transmission in order to achieve .

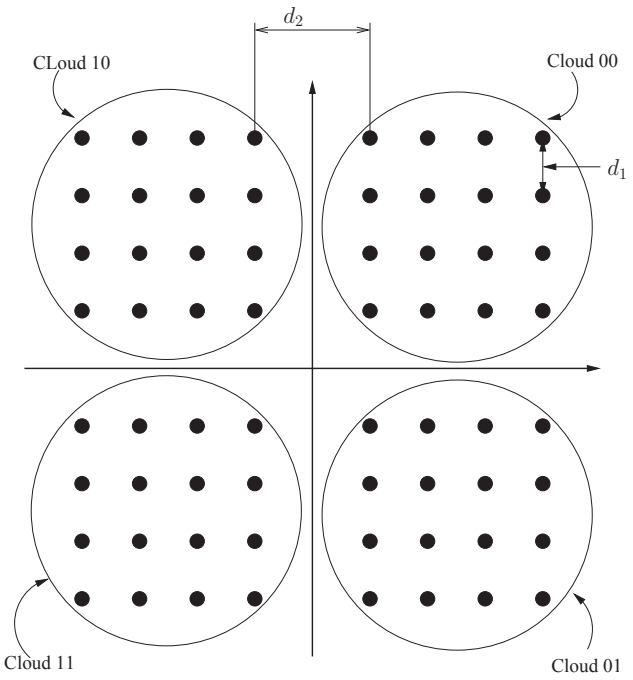

Figure 2.2: MR Modulation using Asymmetric 64-SQAM

We will apportion approximation bits as High Priority (HP) bits and Low Priority (LP) bits according to our modulation scheme design. For 64-ary QAM, each symbol contains 6 bits. After the apportioning, upper 2 bits of the 6 bits are considered as HP bits and mapped into clouds. By creating UEP, the HP bits have better protection from channel errors hence lower BER and LP bits have lower error protection hence higher BER.

2.2 Asymmetric Modulation Scheme Design

In recent years, there has been an increased research towards power and bandwidth efficient modulation scheme design for UEP. For multimedia transmission, where different portion of the compressed source exhibits different levels of importance, modulation scheme with unequal protection is needed. In 2011, such a modulation framework was presented by Hiten and Ilow [7] where the well-known 16-SQAM was used

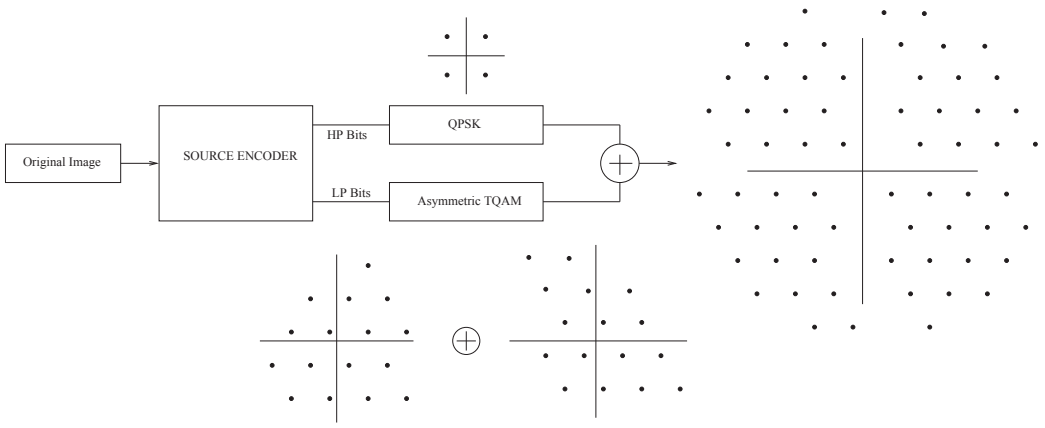

Figure 2.3: MR Modulation using Asymmetric 64-TQAM

for UEP. In [7] UEP was created by mapping different bits with different priority on symbols which are placed on a square grid with unequal vertical and horizontal spacing. However, despite of the easy detection method, 16-SQAM is not optimum in terms of energy efficiency.

In 2007, Sung-Joon Park proposed Triangular Quadrature Amplitude Modulation (TQAM) [26] for Equal Error Protection (EEP), which has better energy efficiency in compare to SQAM with low complexity for detection. In this thesis, we propose a design for asymmetric TQAM with optimum energy efficiency and bit mapping strategy for UEP. In figure 2.4, an asymmetric 64-ary TQAM with UEP is proposed. It is worth observing here that unlike in the asymmetric 64-SQAM where the signalling points are placed on a square grid, in the asymmetric 64-TQAM constellation proposed in this section, signalling points are placed at the vertexes of contiguous equilateral triangles and also spaced at points with co-ordinates different from the conventional scheme resulting in unequal inter-distances between adjacent symbols.

2.2.1 Average Energy Per Symbol Calculation

Asymmetric constellations have different inter-symbol Euclidean distances which allow us to build a hierarchical modulation system and to protect important parts of

the data better by organizing the modulation space properly. For M-ary QAM, each symbol has m number of bits (m is an integer) where, $2^m = M$. In our scenario for 64-ary QAM, where each symbol has $log_2(64) = 6$ bits, we organized the modulation space in such a way that upper 2 bits (HP bits) in each symbol are separated with larger minimum distance and lower 4 bits (LP bits) in each symbol are separated with smaller minimum distance. As we have one third of the bits in each symbol with higher protection, and the rest of the bits with lower protection from errors, one third of the most significant approximation data are mapped into HP bits and the remaining approximation data are mapped into LP bits. In both figure 2.4 and figure 2.5 which represents asymmetric 64-ary TQAM and asymmetric 64-ary SQAM respectively,the bits b_0 and b_1 represent HP bits, while b_2, b_3, b_4 and b_5 represents the LP bits. As mentioned earlier, HP bits are separated horizontally by a larger Euclidean distance ($d_{HP} = 2d$) and LP bits are separated with a smaller Euclidean distance ($d_{LP} = d$). However, considering the worst case scenario, the minimum distance should be the separating distance between points A and C as this distance is smaller than the distance between points B and C. The distance between points A and C is calculated using the law of cosine as,

$$\begin{aligned} AC^2 &= BC^2 + BA^2 - 2 \cdot BC \cdot BA \cdot Cos60 \\ &= d^2 \cdot (4 + 1 - 2) \\ &= 3d^2 \\ &\Rightarrow AC = d \cdot \sqrt{3} \end{aligned} \tag{2.1}$$

Hence, the minimum distance between HP bits is considered as $d_{min}^{HP} = 1.73d$ instead of 2d and minimum distance for LP bits is still $d_{min}^{LP} = d$. Assuming equiprobable symbols, average energy per symbol, E_s, is calculated as $E_s = \frac{1}{M} \sum_{i=1}^{M} E_i$ where E_i is the energy of individual symbols. The energy of the symbols can be obtained as the square of their distances from the origin in the constellation.

The asymmetric 64-TQAM designed in this work is showed in figure 2.4. We can see in the figure that unlike SQAM where signalling points are placed at the vertexes

of squares, in asymmetric 64-TQAM showed in figure 2.4, the signalling points are placed at the vertexes of equilateral triangles, and thus providing more compact and energy efficient structure in compare to asymmetric 64-SQAM. Overall average energy per symbol needed for transmission is calculated similarly as for asymmetric 64-SQAM and found to be

$$E_{tqam} = 12.5625d^2 \tag{2.2}$$

The detail calculation of average energy per symbol using Matlab is presented in Appendix A. where $'d'$ is the smaller inter-symbol minimum distance and is equal to the smaller minimum distance for asymmetric 64-SQAM. This triangular structure has two different minimum distances between adjacent symbols according to priority of error protection. Because minimum distance for HP and LP bits are $d_{min}^{HP} = 1.73d$ and $d_{min}^{LP} = d$ respectively, we can write equation(2.2) in terms of d_{HP} and d_{LP} as,

$$E_{tqam} = 4.1875{d_{min}^{HP}}^2 \tag{2.3}$$

$$E_{tqam} = 12.5625{d_{min}^{LP}}^2 \tag{2.4}$$

Where E_{tqam} represents average energy per symbol for asymmetric 64-TQAM. In equation(1.15), the term M_{min} is the number of neighboring symbols, for each symbol, which are situated at the minimum distance. Since HP bits are mapped as QPSK, so for HP bits, M_{min}=2. On the other hand, LP bits are mapped as asymmetric 16-TQAM, where each symbol has 6 neighboring symbols, which are situated at the minimum distance. As a result, for LP bits, M_{min}=6. According to equation 1.15, SER for HP and LP bits can be written as

$$Pe_{tqam}^{HP} \simeq \frac{2}{2} \cdot \text{erfc}\Big(\sqrt{\frac{E_{tqam}}{N_0}\frac{1}{16.75}}\Big) \tag{2.5}$$

$$Pe_{tqam}^{LP} \simeq \frac{6}{2} \cdot \text{erfc}\Big(\sqrt{\frac{E_{tqam}}{N_0}\frac{1}{50.25}}\Big) \tag{2.6}$$

In the same way BER can be calculated for both HP and LP bits using equation(1.16) as

$$BER_{tqam}^{HP} \simeq \frac{1}{2}Pe_{tqam}^{HP} \tag{2.7}$$

$$BER_{tqam}^{LP} \simeq \frac{1}{4} Pe_{tqam}^{LP} \tag{2.8}$$

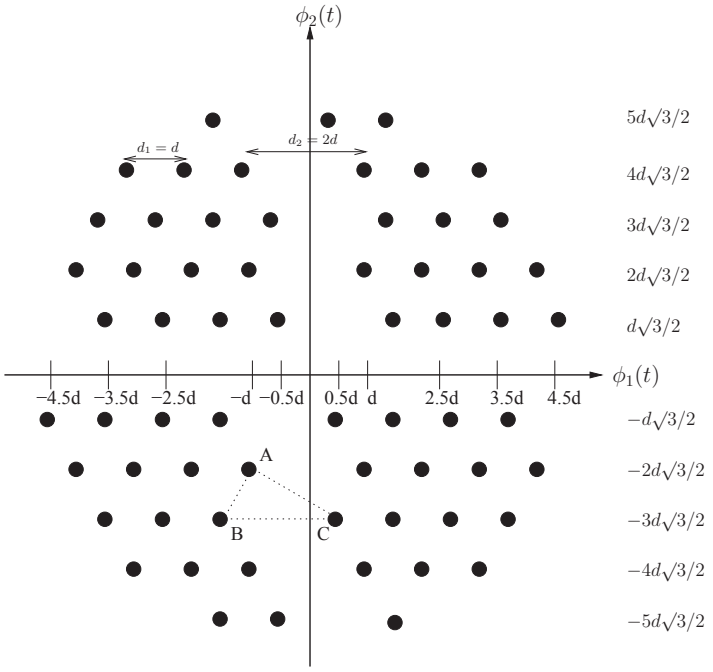

Figure 2.4: Asymmetric 64-ary-TQAM

In asymmetric 64-SQAM, showed in figure 2.5, the signalling points are situated at the vertexes of squares. Number of bits per symbol is $log_2(64) = 6$. If we recall figure 2.4, the minimum distance between HP bits were $d_{min}^{HP} = 1.73d$, while, LP bits (b_2, b_3, b_4 and b_5) are protected with a smaller minimum distance $d_{min}^{LP} = d$. Overall average energy per symbol is calculated as below

$$E_{sqam} = 13.6962d^2 \tag{2.9}$$

Thus using the relation $d_{min}^{HP} = 1.73$d and $d_{min}^{LP} =$ d, The average energy per symbol can be written in terms of d_{HP} and d_{LP} as,

$$E_{sqam} = 4.5671 {d_{min}^{HP}}^2 \tag{2.10}$$

$$E_{sqam} = 13.6962 {d_{min}^{LP}}^2 \tag{2.11}$$

According to equation(1.15), SER for HP and LP bits can be written as

$$Pe_{sqam}^{HP} \simeq \frac{2}{2} \cdot \text{erfc}\Big(\sqrt{\frac{E_{sqam}}{N_0}\frac{1}{18.2686}}\Big) \tag{2.12}$$

$$Pe_{sqam}^{LP} \simeq \frac{4}{2} \cdot \text{erfc}\Big(\sqrt{\frac{E_{sqam}}{N_0}\frac{1}{54.7848}}\Big) \tag{2.13}$$

BER can be calculated for both HP and LP bits using equation(1.16) as

$$BER_{sqam}^{HP} \simeq \frac{1}{2} Pe_{sqam}^{HP} \tag{2.14}$$

$$BER_{sqam}^{LP} \simeq \frac{1}{4} Pe_{sqam}^{LP} \tag{2.15}$$

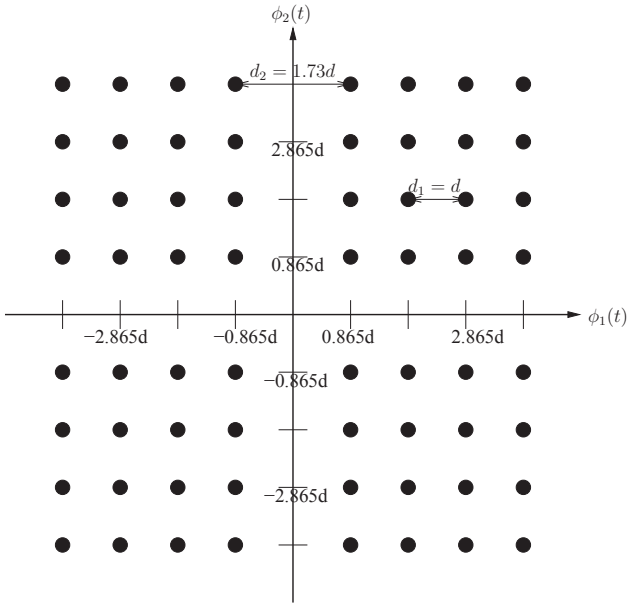

Figure 2.5: Asymmetric 64-ary-SQAM

To get the same order of magnitude in terms of BER, on both HP and LP bits, average energy in equation(2.5), (2.12) and (2.6), (2.13) satisfy the relations,

$$\frac{E_{tqam}}{N_0}\frac{1}{16.75} = \frac{E_{sqam}}{N_0}\frac{1}{18.2686} \tag{2.16}$$

$$\frac{E_{tqam}}{N_0}\frac{1}{50.25} = \frac{E_{sqam}}{N_0}\frac{1}{54.7848} \tag{2.17}$$

The Power Gain (PG) on dB scale of asymmetric 64-TQAM over asymmetric 64-SQAM is calculated as,

$$\begin{aligned} PG &= 10 \cdot log_{10} \frac{E_{sqam}}{E_{tqam}} \\ &= 10 \cdot log_{10} \frac{18.2686}{16.75} = 10 \cdot log_{10} \frac{54.7848}{50.25} \\ &\simeq 0.375 dB \end{aligned} \tag{2.18}$$

As a result of calculation, the asymmetric 64-TQAM provides 0.375 dB overall power gain over the asymmetric 64-SQAM. In the conventional constellations, all bits are equally protected so we have only one BER. However, in asymmetric constellations, for example, in asymmetric 64-SQAM and asymmetric 64-TQAM, we have created different priorities for different bits by adjusting different inter-symbol separation distances and hence we have two different BERs.

We can denote SNR per symbol as γ_s on a linear scale, where $\gamma_s = \frac{E_s}{N_o}$ with E_s is the average energy per symbol. we can write BER for asymmetric 64-SQAM and asymmetric 64-TQAM as

$$BER_{sqam}^{HP} \simeq \frac{1}{2} Pe_{sqam}^{HP} \simeq \frac{1}{2} \cdot \text{erfc}\Big(\sqrt{\gamma_{sqam} \frac{1}{18.2686}}\Big) \tag{2.19}$$

$$BER_{sqam}^{LP} \simeq \frac{1}{4} Pe_{sqam}^{LP} \simeq \frac{1}{2} \cdot \text{erfc}\Big(\sqrt{\gamma_{sqam} \frac{1}{54.7848}}\Big) \tag{2.20}$$

$$BER_{tqam}^{HP} \simeq \frac{1}{2} Pe_{tqam}^{HP} \simeq \frac{1}{2} \cdot \text{erfc}\Big(\sqrt{\gamma_{tqam} \frac{1}{16.75}}\Big) \tag{2.21}$$

$$BER_{tqam}^{LP} \simeq \frac{1}{4} Pe_{tqam}^{LP} \simeq \frac{3}{4} \cdot \text{erfc}\Big(\sqrt{\gamma_{tqam} \frac{1}{50.25}}\Big) \tag{2.22}$$

Where γ_{sqam} and γ_{tqam} represent SNR for asymmetric 64-SQAM and asymmetric 64-TQAM respectively. Equation(2.22) assumes that we have Gray mapping. However, for asymmetric 64-TQAM, perfect Gray mapping is not possible and hence we expect some performance degradation in the BER for LP bits for asymmetric 64-TQAM.

For minimum horizontal distance ratio 4:1, the minimum distance, d_{min} is calculated in the same way as for ratio 2:1. In figure(2.4), for ratio 4:1, BC=4. So, using the law of cosine,

$$\begin{aligned} AC^2 &= BC^2 + BA^2 - 2 \cdot BC \cdot BA \cdot Cos60 \\ &= d^2 \cdot (16 + 1 - 4) \\ &= 13d^2 \\ &\Rightarrow AC = d \cdot \sqrt{13} \end{aligned} \tag{2.23}$$

So, the vertical distance between HP bits is 4d, but minimum distance is $d_{min}^{HP} = 3.6d$, while d_{min}^{LP} = d. The calculation of average energy per symbol for asymmetric 64-TQAM is showed in details in appendix A using Matlab. The average energy per symbol as a result of calculation for the ratio 4:1 is,

$$E_{tqam} = 23.1366d^2 \tag{2.24}$$

Using the relation d_{min}^{HP} = 3.6d and d_{min}^{LP} = d, we can write the average energy per symbol as,

$$E_{sqam} = 1.77{d_{min}^{HP}}^2 \tag{2.25}$$

$$E_{sqam} = 23.1366{d_{min}^{LP}}^2 \tag{2.26}$$

The SER for asymmetric 64-TQAM for the ratio $d_{HP} : d_{LP} = 4 : 1$ can be written as,

$$Pe_{tqam}^{HP} \simeq \frac{2}{2} \cdot \text{erfc}\Big(\sqrt{\frac{E_{tqam}}{N_0}\frac{1}{7.08}}\Big) \tag{2.27}$$

$$Pe_{tqam}^{LP} \simeq \frac{6}{2} \cdot \text{erfc}\Big(\sqrt{\frac{E_{tqam}}{N_0}\frac{1}{92.54}}\Big) \tag{2.28}$$

On the other hand, for asymmetric 64-SQAM, for the ratio $d_{HP} : d_{LP} = 4 : 1$, average energy per symbol is calculated as,

$$E_{tqam} = 24.3170d^2 \tag{2.29}$$

The SER for asymmetric 64-SQAM can be written as,

$$Pe_{sqam}^{HP} \simeq \frac{2}{2} \cdot \text{erfc}\Big(\sqrt{\frac{E_{sqam}}{N_0}\frac{1}{7.48}}\Big) \tag{2.30}$$

$$Pe_{sqam}^{LP} \simeq \frac{4}{2} \cdot \mathrm{erfc}\Big(\sqrt{\frac{E_{sqam}}{N_0}\frac{1}{97.268}}\Big) \tag{2.31}$$

In the same way, SER for asymmetric 64-TQAM and for asymmetric 64-SQAM for the ratio $d_{HP} : d_{LP} = 6 : 1$ can be written as,

$$Pe_{tqam}^{HP} \simeq \frac{2}{2} \cdot \mathrm{erfc}\Big(\sqrt{\frac{E_{tqam}}{N_0}\frac{1}{4.84}}\Big) \tag{2.32}$$

$$Pe_{tqam}^{LP} \simeq \frac{6}{2} \cdot \mathrm{erfc}\Big(\sqrt{\frac{E_{tqam}}{N_0}\frac{1}{150.25}}\Big) \tag{2.33}$$

$$Pe_{sqam}^{HP} \simeq \frac{2}{2} \cdot \mathrm{erfc}\Big(\sqrt{\frac{E_{sqam}}{N_0}\frac{1}{5.06}}\Big) \tag{2.34}$$

$$Pe_{sqam}^{LP} \simeq \frac{6}{2} \cdot \mathrm{erfc}\Big(\sqrt{\frac{E_{sqam}}{N_0}\frac{1}{156.81}}\Big) \tag{2.35}$$

Given that, for 6:1, the minimum distance $d_{min}^{HP} = d \cdot \sqrt{31}$ and $d_{min}^{LP} = \mathrm{d}$. The average energy per symbol is calculated as,

$$E_{tqam} = 37.5625d^2 \tag{2.36}$$

$$E_{sqam} = 39.2033d^2 \tag{2.37}$$

2.2.2 Bit Stream Mapping

When using a higher order modulation scheme, it is necessary to map a binary bit stream into modulation symbols to be transmitted in an optimum manner. The well known 64-SQAM uses Gray mapping, where only one bit differs between adjacent signal points to minimize the number of bits in error. However, perfect Gray mapping for asymmetric 64-TQAM is not possible since there are six adjacent neighbors around almost every signal point, not four neighbors as in the 64-SQAM.

Considering the nature of our UEP scenario, the bit stream mapping is done in such a way that HP bits are mapped as perfect Gray coding, while mapping for LP bits is optimized to ensure minimum Gray coding penalty. Figure 2.6 shows the bit mapped signal points of asymmetric 64-TQAM. Among 6 bits in each symbol, the

upper 2 bits, or red bits, represent HP bits. All symbols in one cloud have the same HP bits or red bits. For example, every symbol in the first cloud is mapped with 00 as the upper 2 bits, while in second, third and fourth cloud, symbols are mapped with 10, 11 and 01 as HP bits, respectively. As this scheme has greater inter-cloud Euclidean distance, HP bits have higher protection from error.

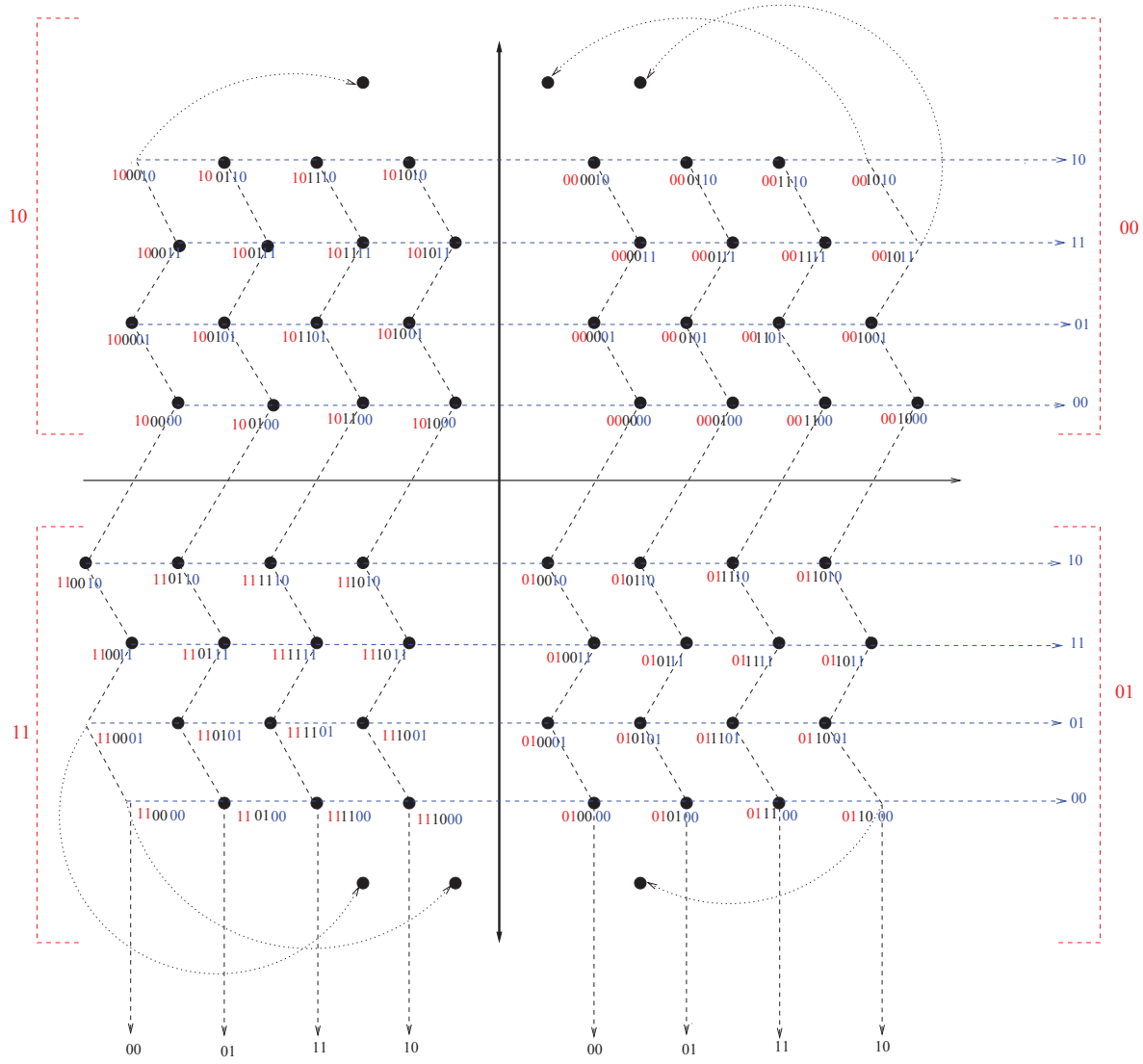

Figure 2.6: Bit mapping of asymmetric 64-ary-TQAM

The lower 4 bits of each signal point represent LP bits and are mapped by their row and column. For example, among lower 4 bits, the upper 2 bits (black bits) are

mapped according to column and lower 2 bits or blue bits are mapped according to row. These bits are mapped with intra-cloud Euclidean distance, which is lower than inter-cloud distance; hence, they have lower protection from error compared with HP bits (red bits). Most of the intra-cloud symbols have six adjacent neighbors, so perfect gray mapping is not possible. However, blue bits in the row and black bits in the column are mapped according to gray mapping to ensure minimum gray mapping penalty for LP bits. Moved or adjusted symbol points are shown with a dotted line, and are mapped according to their original position before moving.

2.3 Simulation results

In this section, we provide simulation results for asymmetric 64-TQAM and compare them with the results from conventional and asymmetric 64-SQAM in terms of symbol error rate (SER) against signal to noise ratio (SNR). Different results from simulation for different minimum distance ratios are presented and comparisons with conventional and asymmetric 64-SQAM are analyzed.

We follow the system model for simulation as shown in figure 2.3. Instead of simulating an entire image, we use random binary numbers. The simulation is done based on the following strategies:

At first, the random binary information is reshaped into groups, each having 6-bits, with the leftmost bit as the most significant bit. The reason for using 6-bits per group is because we are using 64-ary QAM as the modulation scheme, which has $log_2(64) = 6$ bits per symbol. As a result, we can treat each group of 6-bits as a symbol.

After bits are grouped, the symbols are then modulated using both conventional and asymmetric 64-QAM and AWGN as the channel error method. The modulation scheme for asymmetric constellations is designed in such a way that the 2 leftmost bits (HP bits) in each symbol have higher protection from error, while the remaining

4 bits (LP bits) have lower protection from error.

Finally, at the receiving end, each symbol is demodulated and the symbol error rate is calculated. Then HP and LP bits are sorted out and compared before and after modulation for bit error rate.

The simulation is carried out for different ratios of minimum distances. Table 2.1 shows the Power Gain (PG) in dB for Asymmetric SQAM and TQAM.

Table 2.1: Power Gains of Asymmetric TQAM over Asymmetric SQAM

	Average Energy Per Symbol, $\frac{E_s}{d^2}$		PG over SQAM (dB)
	Asymmetric SQAM	Asymmetric TQAM	
$d_2 : d_1$	Overall	Overall	Overall
2:1	13.6962	12.5625	0.375
4:1	24.3170	23.1366	0.216
6:1	39.2033	37.5625	0.186

In table 2.1, the first column indicates the ratios of minimum distances for HP and LP bits ($d_{HP} : d_{LP}$). For example, we have considered 2:1, 4:1 and 6:1 as the minimum distance ratios for table 2.1. The following 2 columns show average energy per symbol ($\frac{E_s}{d^2}$) for asymmetric SQAM and asymmetric TQAM. The last column is showing PG of asymmetric TQAM over asymmetric SQAM.

From the PG values in table 2.1 it is obvious that as the ratio increases from 2:1 to 6:1, the PG decreases. This behavior can be explained by the fact that, increasing minimum distance ratio results in increasing the distance between symbols and the center, and hence decreasing average energy per symbol. PG of asymmetric TQAM over asymmetric SQAM also decreases as the ratio goes from 2:1 to 6:1.

The SER vs SNR curves from theoretical equations are presented for the minimum distance ratio, $d_{HP} : d_{LP}$= 2:1, $d_{HP} : d_{LP}$= 4:1 and $d_{HP} : d_{LP}$= 6:1 in figure 2.7, 2.8 and 2.9 respectively. We used the following equations for ratio 2:1 for the curve in

figure 2.7,

$$Pe_{tqam}^{HP} \simeq \frac{2}{2} \cdot \text{erfc}\Big(\sqrt{\frac{E_{tqam}}{N_0}\frac{1}{16.75}}\Big) \tag{2.38}$$

$$Pe_{tqam}^{LP} \simeq \frac{6}{2} \cdot \text{erfc}\Big(\sqrt{\frac{E_{tqam}}{N_0}\frac{1}{50.25}}\Big) \tag{2.39}$$

$$Pe_{sqam}^{HP} \simeq \frac{2}{2} \cdot \text{erfc}\Big(\sqrt{\frac{E_{sqam}}{N_0}\frac{1}{18.2686}}\Big) \tag{2.40}$$

$$Pe_{sqam}^{LP} \simeq \frac{6}{2} \cdot \text{erfc}\Big(\sqrt{\frac{E_{sqam}}{N_0}\frac{1}{54.7848}}\Big) \tag{2.41}$$

Similarly, for ratio 4:1 and 6:1, we got the curves from theoretical equations and are showed in figure 2.8 and 2.9.

We can observe from the curves that HP bits undoubtedly have the best SER for a certain SNR when compared with LP bits or conventional 64-SQAM. The performance of asymmetric TQAM over asymmetric SQAM in terms of HP bits is always better according to the results. However, as the ratio $d_{HP} : d_{LP}$ increases from 2:1 to 6:1, the performance of both HP and LP bits decreases. For example, when $d_{HP} : d_{LP}$=2:1, for SNR= 28 dB, BER for asymmetric TQAM and SQAM for HP bits is 1.17×10^{-23} and 1.47×10^{-16} respectively, and for LP bits BER is 8.97×10^{-7} and 2.68×10^{-6}. As the ratio increases to 4:1, BER for HP bits is 6.60×10^{-50} for asymmetric TQAM and 8.63×10^{-39} for asymmetric SQAM. While for LP bits BER is 3.9×10^{-4} for asymmetric TQAM and 5.7×10^{-4} for asymmetric SQAM.

We can observe that although BER decreases for both HP and LP bits as the ratio $d_{HP} : d_{LP}$ increases, the performance of asymmetric TQAM decreases compared to asymmetric SQAM. This scenario can be explained by the fact that increasing minimum distance ratio results in increasing the distance between HP bits only, while the separation between LP bits remains the same. Because higher separation between symbols results in lower BER, we observe lower BER for HP bits as the minimum distance ratio increases. However, increasing the ratio also results in greater distance between the center and symbols, and hence decreasing overall power gain, as seen in table 2.1. Because increasing the ratio does not affect the separation between LP bits,

the performance of LP bits decreases as ratio increases. For example, for SNR=28 dB, and for ratio 6:1, BER for LP bits are the same for asymmetric TQAM and asymmetric SQAM.

In figure 2.7, 2.8 and 2.9 the SER bs SNR curve is plotted using the theoretical calculation of SER. However, from the theoretical SER, we can also get the BER for HP and LP bits using the relation from equation(2.14) and (2.15). In this thesis, we have also verified the BER using Matlab simulation. The code and results for BER using Matlab simulation is presented in appendix B. Table 2.2 shows the BER from theoretical calculation and from Matlab simulation for certain SNR values.

Table 2.2: BER from Theoretical Calculation vs Matlab Simulation for ratio 2:1

SNR (dB)	Theoretical BER (HP bits)	Simulation BER (HP bits)	Theoretical BER (LP bits)	Simulation BER (LP bits)
18	7.4×10^{-3}	7.8×10^{-4}	6.1×10^{-2}	6.20×10^{-2}
20	5.49×10^{-4}	6×10^{-5}	2.3×10^{-2}	2.7×10^{-2}
22	1.23×10^{-5}	1×10^{-5}	5.75×10^{-3}	7.3×10^{-3}

From table 2.2, we can see that for LP bits, the BER for theoretical calculation and from Matlab simulation is approximately the same. On the other hand, for HP bits, for some certain SNRs (for example, when SNR = 18 dB and 20 dB), The BER from simulation is better than BER from theoretical calculation. These results can be explained by the fact that, using theoretical calculation we always assume the minimum distance $d_{HP} = 1.73d$ which is for the worst case scenario. However, in practical case, we do not always have the worst case scenario of the minimum distance. As a result, using Matlab simulation sometime has better performance in terms of BER.

Thus we can conclude that increasing minimum distance ratio decreases BER for both HP and LP bits. However, increasing the ratio also means there separation between the center and symbols getting higher and hence the average energy per symbol will also be higher compared to the other ratios.

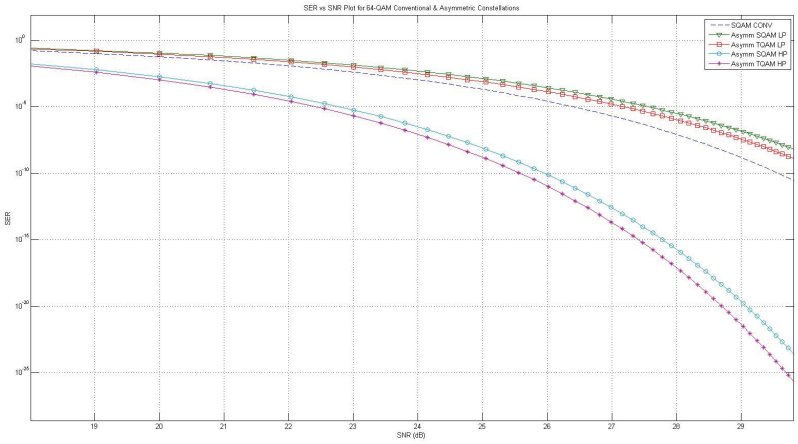

Figure 2.7: SER vs SNR curve for $d_{HP} : d_{LP} = 2{:}1$

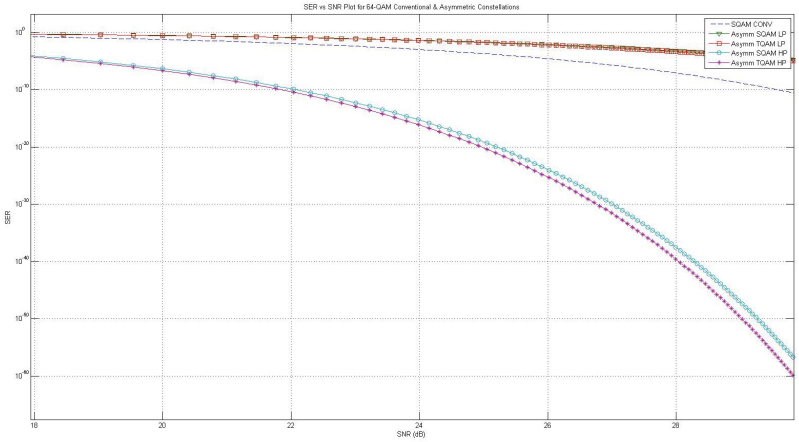

Figure 2.8: SER vs SNR curve for $d_{HP} : d_{LP} = 4{:}1$

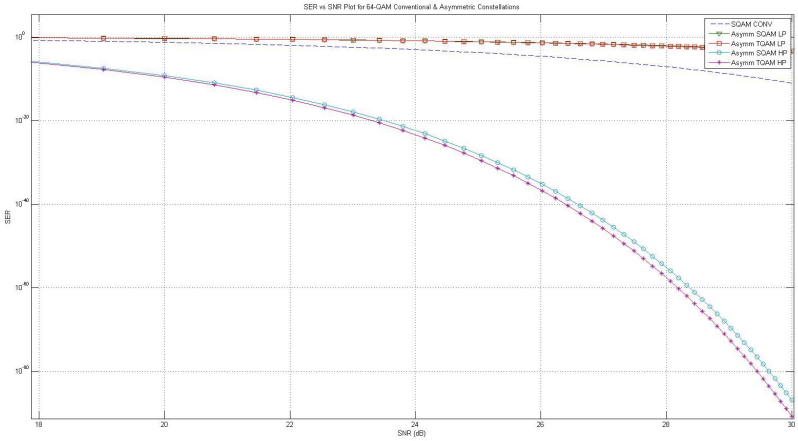

Figure 2.9: SER vs SNR curve for $d_{HP} : d_{LP} = 6{:}1$

Chapter 3

Image Transmission Results using 64-ary Asymmetric TQAM

In order to store and transmit images in a more efficient way, compression techniques are required. Compression of image data is achieved by removing the correlation among the pixels as in predictive coding. The process of DWT of a signal is essentially a process of performing decorrelation of the signal, and thereby compacting the energy which is spread across the signal in its original domain to a few coefficients in the transform domain. Typically images exhibit strong correlation among neighboring pixels, giving rise to redundancy of information. DWT helps remove this information redundancy, and thereby compact the energy of the image signal to few coefficients in the transform domain. Thus, the DWT coefficients with less energy can be ignored without significantly affecting the image quality. This method of compression can be termed as lossy compression as we introduce information loss, however insignificant, while reconstruction [7].

In this chapter, we will discuss about the image transmission framework adopted in this research in section 3.1. Quantization is described in chapter 3.2. Then the results for image transmission in terms of PSNR is presented in section 3.3 followed by simulation results of lena image for different SNR.

3.1 DWT Based Image Transmission

The image transmission scenario used in this research is based on 2D-DWT and showed in figure 1.4. The image is a 512×512 Lena image showed in figure 3.1.

Figure 3.1: Original 512×512 Lena image

So, after one level of decomposition using 2D-DWT, we will have four portions of subbands each having the same size 256×256. As described earlier, in this research we only transmit the coarse information which is the LL subband. An square image of dimension 512×512 pixels would require a maximum of 9 bits for representation. Then we need 1 level DWT decomposition to get subbands of size 256×256 pixels. The LL subband, as described details in section 1.1.4, consists of information according to importance in a zigzag manner. Hence, we apply a zigzag matrix along the LL subband to sort the wavelet decomposition coefficients in an one dimensional matrix of size 1×65536. This matrix has coefficients from left to right of priority higher to lower. We are using 64-QAM as modulation scheme which has 6 bits per symbol among which 2 bits are reserved for HP bits and the rest 4 bits are for LP bits. Because one third of the bits in a symbol are reserved for HP bits, first one third of the coefficients, or in other word, one-third of the high priority coefficients are

mapped into HP bits. The rest of the coefficients are mapped into LP bits.

For simulating transmission errors we used Binary Symmetric Channel (BSC) showed in figure 3.2.

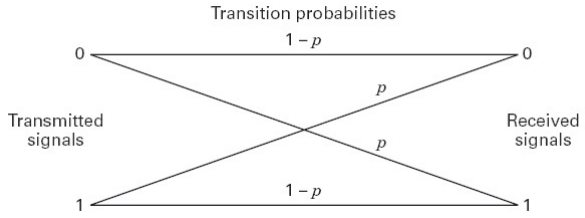

Figure 3.2: Binary Symmetric Channel

BSC is a channel with binary input and binary output with a crossover probability of error p. Because we have two different groups of bits with different probability of error, we used two separate BSC with different probability of error. The BER to be used in this image transmission framework is listed in table 3.1, 3.2 and **??**. After the image has been transmitted through BSC, HP and LP bits are concatenated to retrieve the entire image. The quality of the received image depends on minimum distance ratio, SNR and BER. Received images are presented in section 3.3.

3.2 Image Quantization

An important aspect of the image coding (or compression) process is **quantization** [28]. Quantization is the process for representing a set of values with a set of codewords used to represent those values [29]. Since, in this research the quantization utilized is for lossy compression, the source coder generated number of possible values is greater than the codewords.

A quantization function at the encoder can be described as follows [30]. Suppose N is the number of a set of intervals and I=1,2,...,N. The boundary values of these intervals are represented by b_l(l=0,1,...,N). The reconstruction values are represented

by g_l(l=1,...,N). Then the ranges of these intervals can be represented as B_l=(b_{l-1}, b_l).

In [30], the quantization function Q_f is defined as,

$$Q_f(x) = g_l \tag{3.1}$$

where $x\epsilon B_l, l\epsilon I$.

A $uniformquantizer$ performs a type of scalar quantization. All of the intervals are the same size.

$$b_i - b_{i-1} = g_i - g_{i-1} = q \tag{3.2}$$

where q is referred as quantization steps. A uniform quantizer is illustrated in figure 3.3.

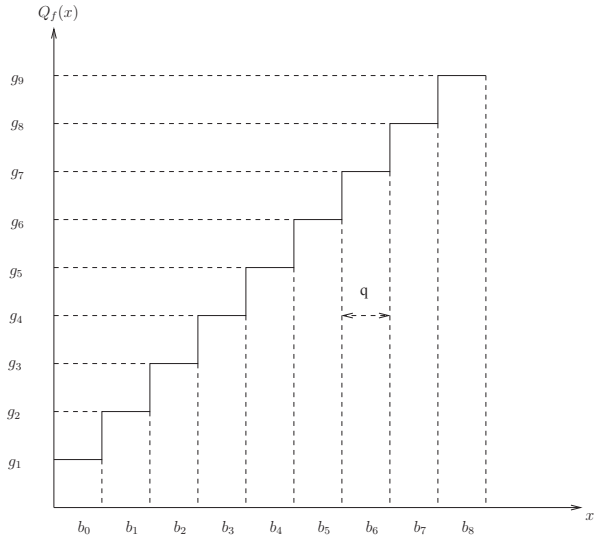

Figure 3.3: Uniform Quantizer

Although there has been a lot of research involving image quantization, the focus of this research is on modulation scheme design for UEP based image transmission. As a result we will be using a general-purpose uniform quantizer to avoid complication.

The process of quantization adopted in this research is explained with the following example. Consider a uniform integer quantizer with 2^{17} = 131072 levels of quantization from -65536 to +65535, and step size of 1 unit. Then, the encoded representation of a coefficient with a value of 64336.98 is simply the binary representation

of the integer portion 64336, which falls within the limits of the quantizer (-65536 to +65535). Thus, the decimal representation of the DWT coefficient is encoded in the binary format as '01111101101010000' with the leading MSB as the sign bit (0 for plus sign, and 1 for minus sign) to account for the sign of the coefficient in addition to its magnitude, which only requires $2^{16} = 65536$ levels of quantization in one direction (positive or negative), and thus only 16 bits for encoding.

3.3 Simulation results

Table 3.1 and 3.2 show the simulation results of BER vs $PSNR$ for the ratio d_{HP} : d_{LP} of 2:1 and 4:1 respectively. We listed BER values for different SNRs using figure 2.7 and 2.8. Then the original 512×512 Lena image showed in figure 3.1 is transmitted using asymmetric TQAM and asymmetric SQAM through a binary symmetric channel. The resulting PSNR is showed in the tables.

Table 3.1: BER and PSNR analysis of Lena image for $d_2 : d_1$=2:1

SNR	BER_{HP}(TQAM)	BER_{HP}(SQAM)	BER_{LP}(TQAM)	BER_{LP}(SQAM)	$PSNR_{TQAM}$ (dB)	$PSNR_{SQAM}$ (dB)
18	7.43×10^{-3}	1×10^{-2}	6.1×10^{-2}	6.9×10^{-2}	23.76	22.94
20	5.495×10^{-4}	9.37×10^{-4}	2.3×10^{-2}	2.8×10^{-2}	28.45	27.28
22	1.23×10^{-5}	2.84×10^{-5}	5.75×10^{-3}	7.7×10^{-3}	34.29	32.62
24	2.71×10^{-8}	9.5×10^{-8}	6.25×10^{-4}	1.02×10^{-3}	40.36	38.47
26	4.81×10^{-12}	3.6×10^{-11}	3.25×10^{-5}	6.5×10^{-5}	41.58	41.38
28	2.29×10^{-18}	5.73×10^{-17}	2.24×10^{-7}	6.7×10^{-7}	41.63	41.63

It is obvious from the PSNR values that, as the SNR increases, there is an increase in the PSNR for all minimum distance ratios. This behavior can be explained by the fact that the increase in CNR implies increase in the average energy of the constellation. This allows inclusion of more symbols in the constellation with same or greater Euclidean distances between symbols. Consequently, with more symbols the receiver has more information to reconstruct the image with better quality (PSNR).

Table 3.2: BER and PSNR analysis of Lena image for $d_2 : d_1$=4:1

SNR	BER_{HP}(TQAM)	BER_{HP}(SQAM)	BER_{LP}(TQAM)	BER_{LP}(SQAM)	$PSNR_{TQAM}$ (dB)	$PSNR_{SQAM}$ (dB)
18	3.83×10^{-5}	6×10^{-5}	0.125	0.125	21.63	21.55
20	1.06×10^{-7}	2.33×10^{-7}	0.07	0.07	24.05	23.87
22	1.78×10^{-11}	6.1×10^{-11}	0.031	0.031	27.51	27.38
24	4.32×10^{-17}	2.94×10^{-16}	0.0099	0.0099	32.18	31.84
26	2.16×10^{-26}	4.56×10^{-25}	0.0016	0.0016	38.26	37.62
28	1.34×10^{-40}	1.61×10^{-38}	0.00011	0.00016	41.34	40.98
30	2.15×10^{-63}	4.22×10^{-60}	0.0000016	0.0000029	41.63	41.63

We can see from table 3.1 that as the SNR increases, the difference between PSNR of asymmetric TQAM and asymmetric SQAM decreases. This behavior can be explained by the fact that, higher values of SNR results in lower BER for HP and LP bits. But the decay of BER for asymmetric SQAM is much more rapid than the decay of asymmetric TQAM. As a result, having higher SNR means the difference between PSNR of asymmetric TQAM and asymmetric SQAM is smaller.

If we consider the parameter-minimum distance ratio ($d_{HP} : d_{LP}$), we can observe that, although BER for HP bits lowers for a certain SNR as the ratio increases, but BER for LP bits rises as the ratio increases. This scenario can be explained by the fact that, increasing the ratio results in bigger distance between HP bits only. As bigger Euclidean distance results in lower BER, we are having lower SNR for HP bits as the ratio increases. For example, if we consider SNR=24 dB, BER for asymmetric TQAM for HP bits are, 2.71×10^{-8} for ratio 2:1 and 4.32×10^{-17} for ratio 4:1.

On the other hand, increasing the ratio doesn't affect the Euclidean distance between LP bits. Because higher ratio means higher distance between center and the symbols, the overall power gain decreases as the ratio increases. As a result, the performance of LP bits in terms of BER decreases as ratio increases.

The reconstructed Lena images are showed in figure 3.4, 3.5 and 3.6 for minimum distance ratio 2:1. In figure 3.4, all the images are reconstructed using 22 dB SNR for transmission. From left to right, 3 images represent reconstructed Lena image using

conventional 64 QAM, asymmetric 64-SQAM and asymmetric 64-TQAM respectively. Corresponding PSNR values are listed at the bottom of each image.

In the figure 3.4, the distortion artifacts occurring due to the errors introduced by channel can be easily seen. Image quality in terms of PSNR improves from conventional SQAM to asymmetric TQAM. The PSNR values proves that asymmetric TQAM provides the best image quality in compare to conventional SQAM and asymmetric SQAM.

Similarly, figure 3.5 and 3.6 shows reconstructed images for SNR = 24 dB and SNR = 26 dB respectively. It is worth observing that the image quality improves for higher SNR which supports our explanation above. Also as the SNR increase from 22 dB to 26 dB, the difference of PSNR value of asymmetric TQAM with conventional and asymmetric SQAM decreases. Figure 3.7 and 3.8 show the SNR vs PSNR

Figure 3.4: Reconstructed images for SNR = 22 dB.

Figure 3.5: Reconstructed images for SNR = 24 dB

Figure 3.6: Reconstructed images for SNR = 26 dB

curve for $d_{HP} : d_{LP}$ = 2:1 and 4:1 respectively. From these figures we can observe that, the performance of asymmetric TQAM over asymmetric SQAM in terms of PSNR decreases as the ratio goes from 2:1 to 4:1. It supports our previous theory that, increasing minimum distance ratio will decrease BER but at the same time it deteriorates the performance in terms of PSNR because of less power gain.

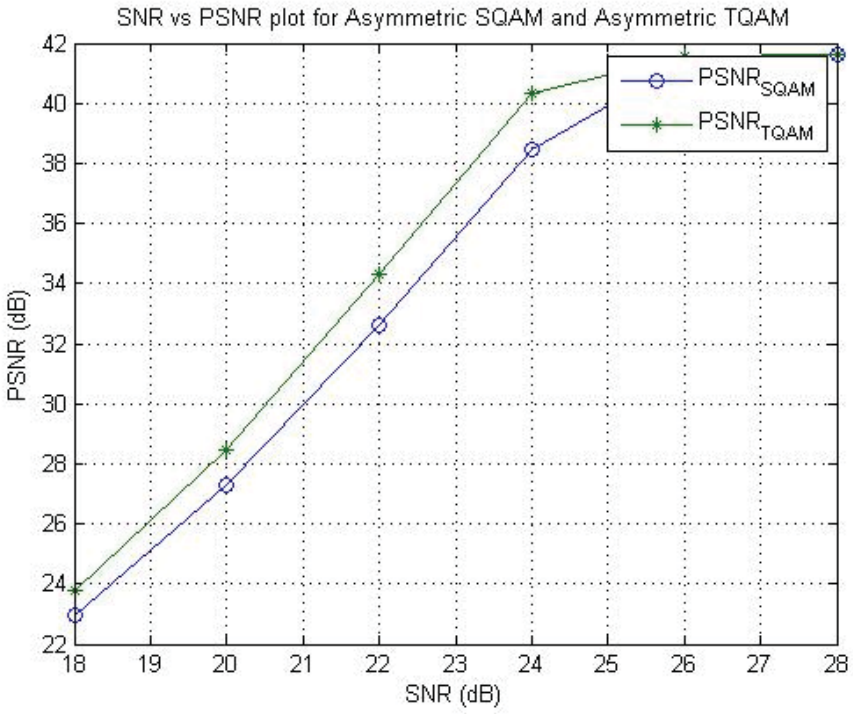

Figure 3.7: SNR vs PSNR curve for $d_{HP} : d_{LP}$=2:1

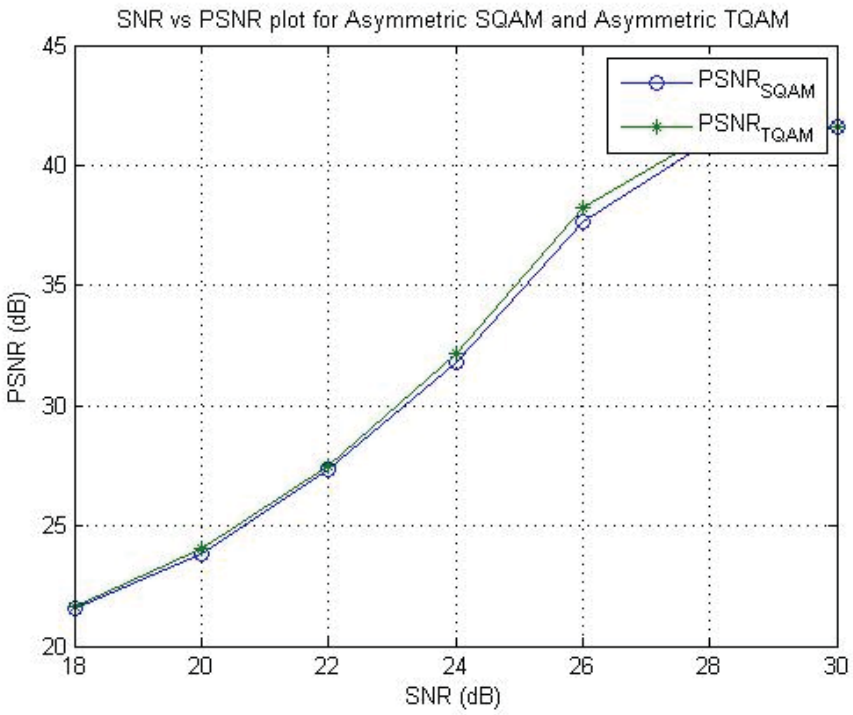

Figure 3.8: SNR vs PSNR curve for $d_{HP} : d_{LP}$=4:1

Chapter 4

Conclusion and Future Research

The joint source channel coding technique proposed in this thesis improved the quality of image transmission framework with the design of asymmetric modulation scheme. This proposed scheme combines UEP with efficient design for power gain, which is of great importance to still image transmission systems (i.e. satellite communications). This chapter summarizes the thesis and suggests potential avenues for future work to further our investigation.

4.1 Thesis Contributions

1. **Modified Triangular QAM for UEP**

   For unequal error protection based image transmission, square QAM is not optimum in terms of energy efficiency. In this research, we designed or in other words modified triangular QAM for UEP based communications. This design was also matched with the technique of MR modulation, where low priority information representing details are superimposed on to high priority approximation information to achieve scalability in UEP based communications which leads to a robust joint source-channel coding framework.

2. **Customized Bit Mapping for LP bits**

Because in the well known square QAM, each symbol has four neighbors, Gray mapping is possible and hence from implementation point of view, SQAM is very popular. However, the asymmetric TQAM designed in this research, each symbol has a maximum of six neighbors which makes it impossible to carry out a perfect Gray mapping. In this research, we designed the bit mapping in such a way that high priority information is mapped according to perfect Gray mapping to ensure best reliability of error free transmission. On the other hand, bit mapping for low priority information is carried out to minimize Gray mapping penalty. As a result, although perfect Gray mapping was not possible for the entire constellation of asymmetric TQAM, our proposed bit mapping strategy protects high priority information by perfect Gray mapping while also ensures low priority information experience minimum Gray mapping penalty.

3. **Joint Source-Channel Coding Framework**

   In this research, we combined multimedia source coding with UEP based MR modulation scheme to propose a robust joint source- channel coding framework for image transmission. The different priority of information was addressed through unequal error protection based asymmetric modulation scheme to match the channel coding method with source coding without using any extra information bit for error protection.

4.2 Future Work

The work done from this thesis, we find areas with future scope of investigation. These areas of future work is described in following:

1. In this thesis, we employed a source coding strategy which is based on transform coding. Also to avoid complication, 2D-DWT was used for source coding. However, more developed image coding schemes such as Said and Pearlman's

SPIHT [17] is scalable and progressive in nature. The strategy in this research can be extended to find new ways of incorporating such new image coding schemes as our proposed UEP framework is suitable for progressive source coding schemes.

2. In our work, we only considered 64-ary QAM as modulation scheme.Our design was primarily based on 4 symbols for HP bits around 16 symbols for LP bits (16-around-4). However, similar design strategy can be adopted for designing asymmetric 256-ary TQAM with 16 symbols for HP bits and 16 symbols for LP bits (16-around-16), and for 1024-ary TQAM with 16 symbols for HP bits and 64 symbols for LP bits (16-around-64). With higher modulation schemes we have mor flexibility of rearranging symbols to design asymmetric constellation and hence higher performance in terms of power gain and bit error rate.

Appendix A
Calculation of Average Energy Per Symbol

This appendix presents the calculation of average energy per symbol for asymmetric 64-TQAM and asymmetric 64-SQAM for different ratios of minimum distances. Theoretically, energy for a symbol in a constellation is calculated by the distance square from the center of the constellation. For example, if co-ordinates for signalling points are $(x_1, y_1), (x_2, y_2) \cdots (x_i, y_i)$ (where i=1,2,3,...,64 for 64-ary QAM), then the average energy per symbol can be calculated by the following equation,

$$E_{avg} = \frac{1}{64} \sum_{i=1}^{64} ({x^2}_i + {y^2}_i) \tag{A.1}$$

Using equation(A.1), we calculated the average energy per symbol for asymmetric 64-TQAM and asymmetric 64-SQAM. For asymmetric 64-TQAM, the calculation in Matlab is showed in the following screenshots A.1 and A.2.

For asymmetric 64-SQAM, the calculation for average energy per symbol is shown below in figures A.3 and A.4

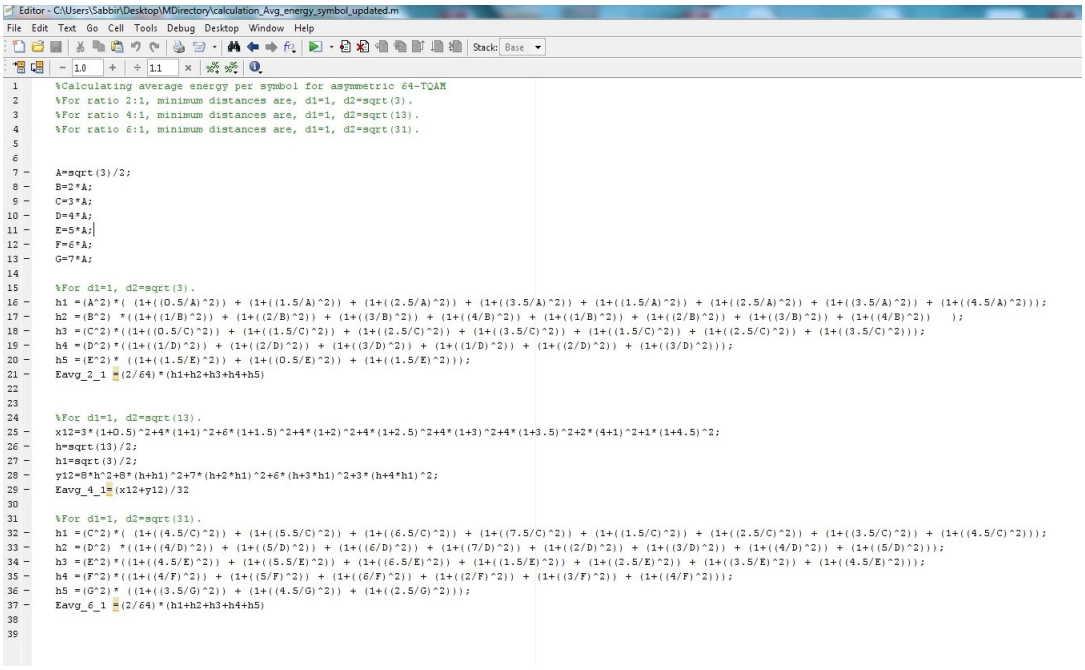

Figure A.1: Average energy per symbol for asymmetric 64-TQAM

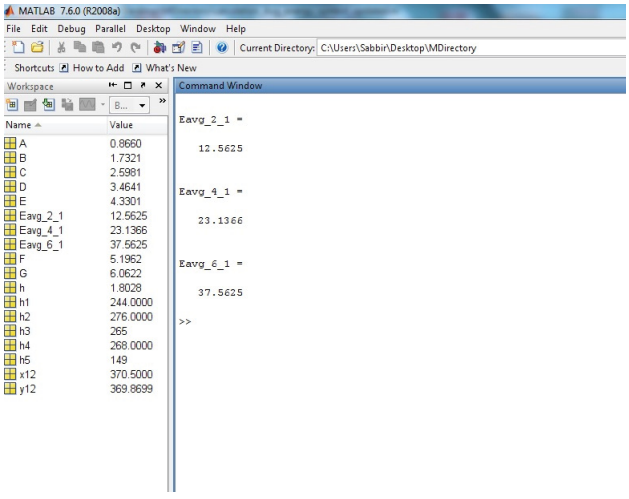

Figure A.2: Average energy per symbol results for asymmetric 64-TQAM

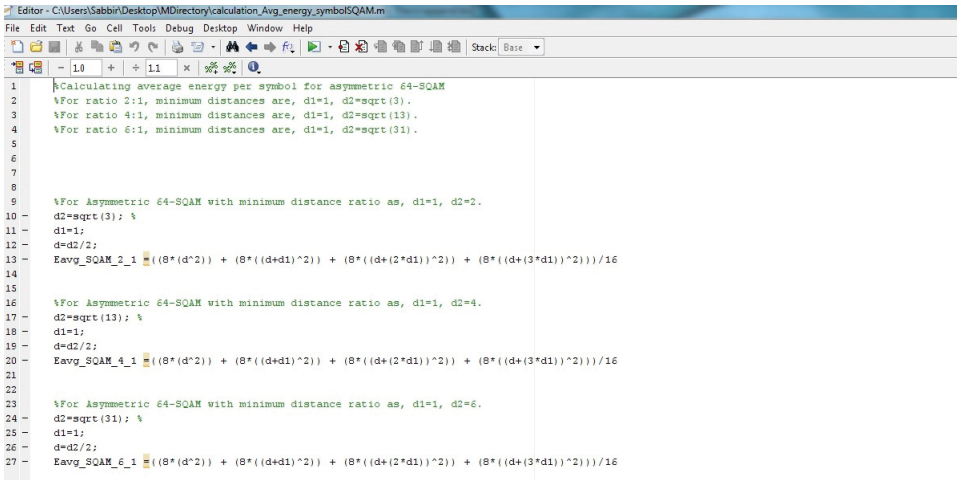

Figure A.3: Average energy per symbol for asymmetric 64-SQAM

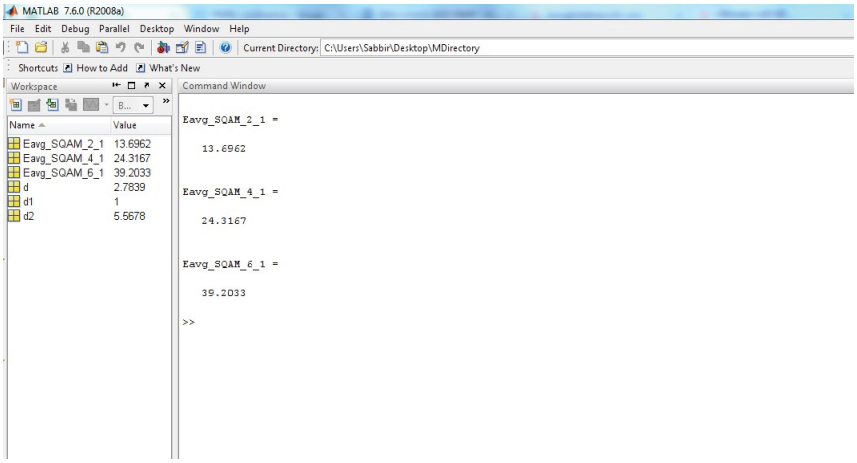

Figure A.4: Average energy per symbol results for asymmetric 64-SQAM

Appendix B

Matlab Simulation Results for BER vs SNR

This appendix presents the Matlab simulation results for BER vs SNR for minimum distance ratio 2:1. Table 2.2 shows the comparison of BER vs SNR results from theoretical equations vs Matlab simulation. Here, we verify the results from Matlab simulation by presenting screenshots of Matlab code as well as results of BER vs SNR. Figure B.5 and B.6 show the simulation results for SNR = 18 dB. While B.7 and B.8 show simulation results for SNR = 20 dB; figure B.9 and B.10 show the results for SNR = 22 dB.

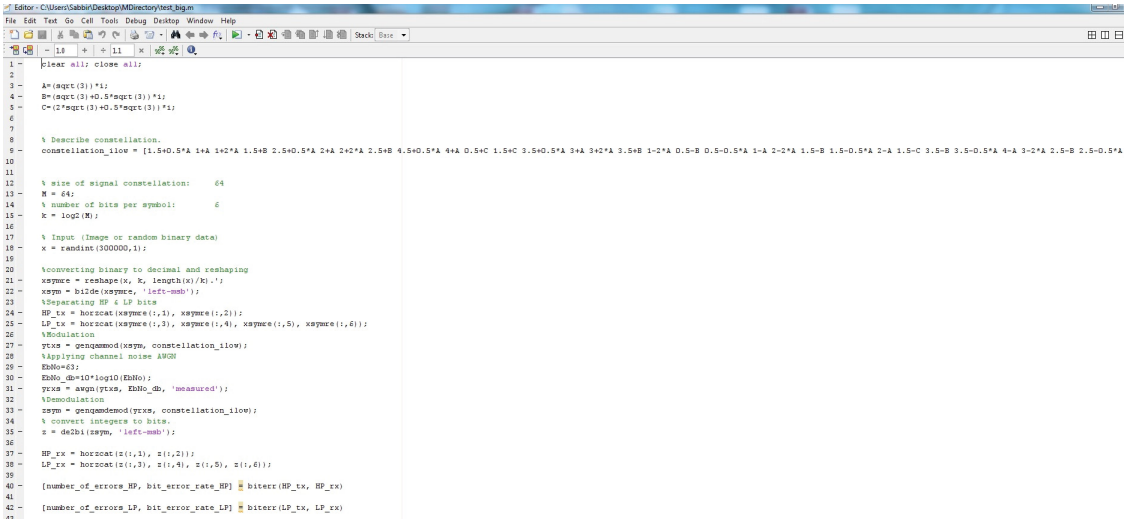

```
clear all; close all;

A=(sqrt(3))*i;
B=(sqrt(3)+0.5*sqrt(3))*i;
C=(2*sqrt(3)+0.5*sqrt(3))*i;


% Describe constellation.
constellation_ilow = [1.5+0.5*A 1+A 1+2*A 1.5+B 2.5+0.5*A 2+A 2+2*A 2.5+B 4.5+0.5*A 4+A 0.5+C 1.5+C 3.5+0.5*A 3+A 3+2*A 3.5+B 1-2*A 0.5-B 0.5-0.5*A 1-A 2-2*A 1.5-B 1.5-0.5*A 2-A 1.5-C 3.5-B 3.5-0.5*A 4-A 3-2*A 2.5-B 2.5-0.5*A


% size of signal constellation:     64
M = 64;
% number of bits per symbol:        6
k = log2(M);

% Input (Image or random binary data)
x = randint(300000,1);

%converting binary to decimal and reshaping
xsymre = reshape(x, k, length(x)/k).';
xsym = bi2de(xsymre, 'left-msb');
%Separating HP & LP bits
HP_tx = horzcat(xsymre(:,1), xsymre(:,2));
LP_tx = horzcat(xsymre(:,3), xsymre(:,4), xsymre(:,5), xsymre(:,6));
%Modulation
ytxs = genqammod(xsym, constellation_ilow);
%Applying channel noise AWGN
EbNo=63;
EbNo_db=10*log10(EbNo);
yrxs = awgn(ytxs, EbNo_db, 'measured');
%Demodulation
zsym = genqamdemod(yrxs, constellation_ilow);
% convert integers to bits.
z = de2bi(zsym, 'left-msb');

HP_rx = horzcat(z(:,1), z(:,2));
LP_rx = horzcat(z(:,3), z(:,4), z(:,5), z(:,6));

[number_of_errors_HP, bit_error_rate_HP] = biterr(HP_tx, HP_rx)

[number_of_errors_LP, bit_error_rate_LP] = biterr(LP_tx, LP_rx)
```

Figure B.5: Matlab Code for BER vs SNR for SNR = 18 dB

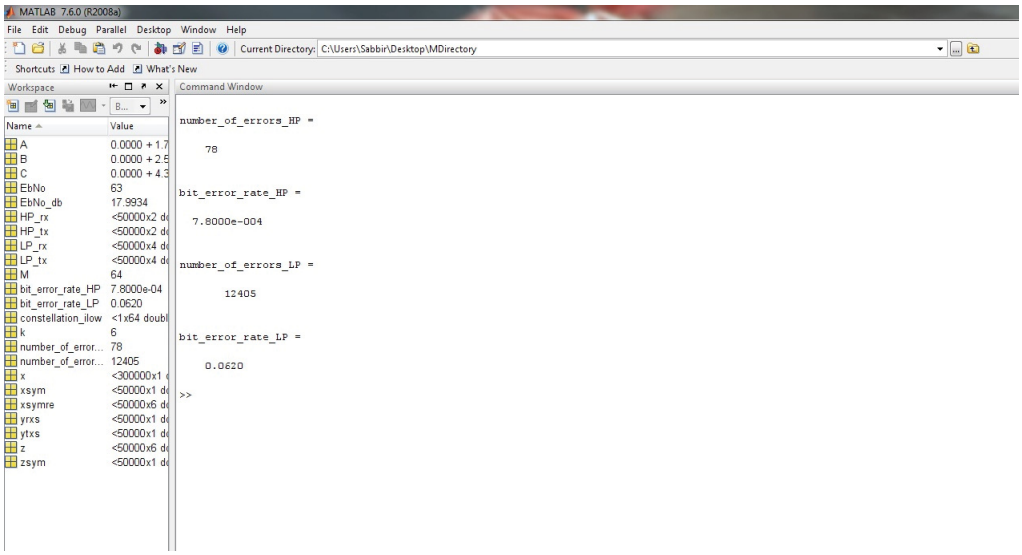

```
MATLAB 7.6.0 (R2008a)
File  Edit  Debug  Parallel  Desktop  Window  Help
Current Directory: C:\Users\Sabbir\Desktop\MDirectory
Shortcuts  How to Add  What's New

Workspace
Name                Value
A                   0.0000 + 1.7
B                   0.0000 + 2.5
C                   0.0000 + 4.3
EbNo                63
EbNo_db             17.9934
HP_rx               <50000x2 d
HP_tx               <50000x2 d
LP_rx               <50000x4 d
LP_tx               <50000x4 d
M                   64
bit_error_rate_HP   7.8000e-04
bit_error_rate_LP   0.0620
constellation_ilow  <1x64 doubl
k                   6
number_of_error...  78
number_of_error...  12405
x                   <300000x1
xsym                <50000x1 d
xsymre              <50000x6 d
yrxs                <50000x1 d
ytxs                <50000x1 d
z                   <50000x6 d
zsym                <50000x1 d

Command Window

number_of_errors_HP =

    78


bit_error_rate_HP =

  7.8000e-004


number_of_errors_LP =

       12405


bit_error_rate_LP =

    0.0620

>>
```

Figure B.6: Simulation Results for BER vs SNR for SNR = 18 dB

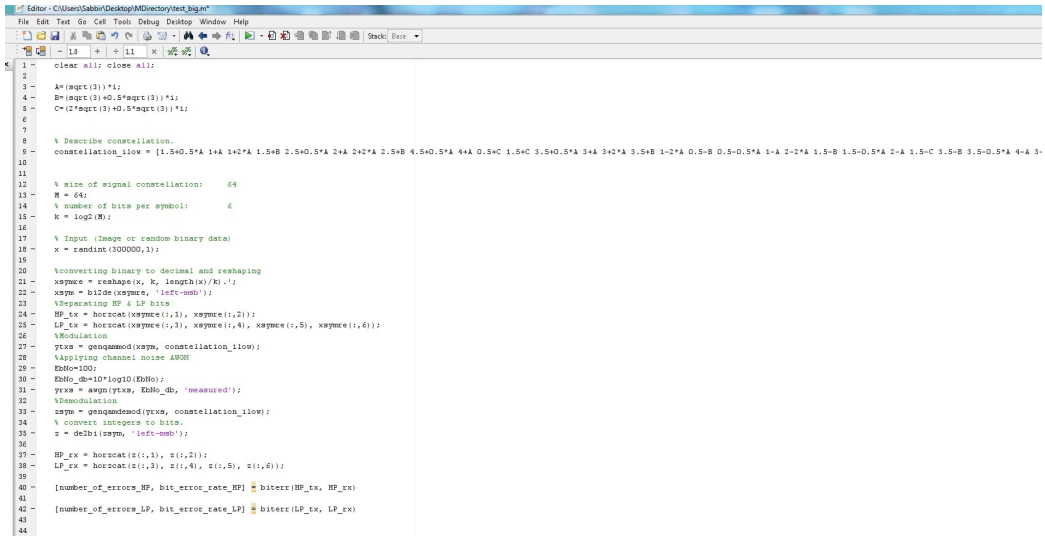

```
clear all; close all;

A=(sqrt(3))*i;
B=(sqrt(3)+0.5*sqrt(3))*i;
C=(2*sqrt(3)+0.5*sqrt(3))*i;


% Describe constellation.
constellation_ilow = [1.5+0.5*A 1+A 1+2*A 1.5+B 2.5+0.5*A 2+A 2+2*A 2.5+B 4.5+0.5*A 4+A 0.5+C 1.5+C 3.5+0.5*A 3+A 3+2*A 3.5+B 1-2*A 0.5-B 0.5-0.5*A 1-A 2-2*A 1.5-B 1.5-0.5*A 2-A 1.5-C 3.5-B 3.5-0.5*A 4-A 3-


% size of signal constellation:     64
M = 64;
% number of bits per symbol:        6
k = log2(M);

% Input (Image or random binary data)
x = randint(300000,1);

%converting binary to decimal and reshaping
xsymre = reshape(x, k, length(x)/k).';
xsym = bi2de(xsymre, 'left-msb');
%Separating HP & LP bits
HP_tx = horzcat(xsymre(:,1), xsymre(:,2));
LP_tx = horzcat(xsymre(:,3), xsymre(:,4), xsymre(:,5), xsymre(:,6));
%Modulation
ytxs = genqammod(xsym, constellation_ilow);
%Applying channel noise AWGN
EbNo=100;
EbNo_db=10*log10(EbNo);
yrxs = awgn(ytxs, EbNo_db, 'measured');
%Demodulation
zsym = genqamdemod(yrxs, constellation_ilow);
% convert integers to bits.
z = de2bi(zsym, 'left-msb');

HP_rx = horzcat(z(:,1), z(:,2));
LP_rx = horzcat(z(:,3), z(:,4), z(:,5), z(:,6));

[number_of_errors_HP, bit_error_rate_HP] = biterr(HP_tx, HP_rx)

[number_of_errors_LP, bit_error_rate_LP] = biterr(LP_tx, LP_rx)
```

Figure B.7: Matlab Code for BER vs SNR for SNR = 20 dB

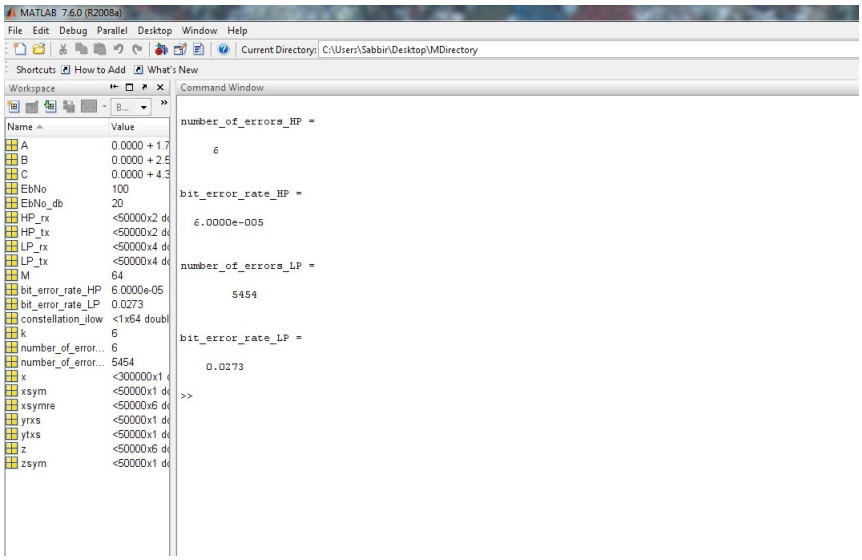

```
MATLAB 7.6.0 (R2008a)
File  Edit  Debug  Parallel  Desktop  Window  Help
Current Directory: C:\Users\Sabbir\Desktop\MDirectory
Shortcuts  How to Add  What's New

Workspace
Name                Value
A                   0.0000 + 1.7
B                   0.0000 + 2.5
C                   0.0000 + 4.3
EbNo                100
EbNo_db             20
HP_rx               <50000x2 d
HP_tx               <50000x2 d
LP_rx               <50000x4 d
LP_tx               <50000x4 d
M                   64
bit_error_rate_HP   6.0000e-05
bit_error_rate_LP   0.0273
constellation_ilow  <1x64 doubl
k                   6
number_of_error...  6
number_of_error...  5454
x                   <300000x1
xsym                <50000x1 d
xsymre              <50000x6 d
yrxs                <50000x1 d
ytxs                <50000x1 d
z                   <50000x6 d
zsym                <50000x1 d

Command Window

number_of_errors_HP =

     6


bit_error_rate_HP =

  6.0000e-005


number_of_errors_LP =

        5454


bit_error_rate_LP =

    0.0273

>>
```

Figure B.8: Simulation Results for BER vs SNR for SNR = 20 dB

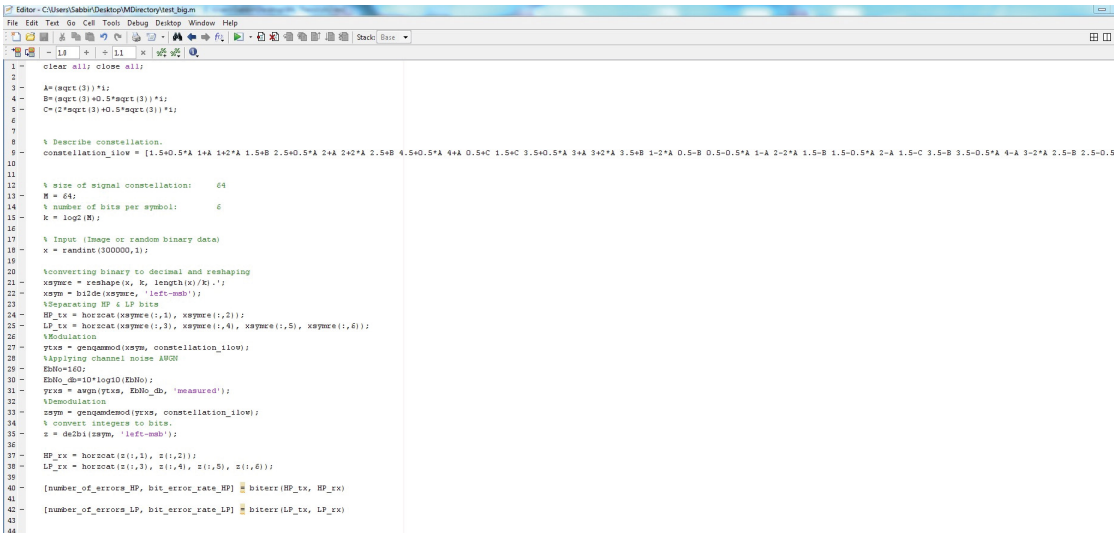

```
clear all; close all;

A=(sqrt(3))*i;
B=(sqrt(3)+0.5*sqrt(3))*i;
C=(2*sqrt(3)+0.5*sqrt(3))*i;


% Describe constellation.
constellation_ilow = [1.5+0.5*A 1+A 1+2*A 1.5+B 2.5+0.5*A 2+A 2+2*A 2.5+B 4.5+0.5*A 4+A 0.5+C 1.5+C 3.5+0.5*A 3+A 3+2*A 3.5+B 1-2*A 0.5-B 0.5-0.5*A 1-A 2-2*A 1.5-B 1.5-0.5*A 2-A 1.5-C 3.5-B 3.5-0.5*A 4-A 3-2*A 2.5-B 2.5-0.5


% size of signal constellation:     64
M = 64;
% number of bits per symbol:        6
k = log2(M);

% Input (Image or random binary data)
x = randint(300000,1);

%converting binary to decimal and reshaping
xsymce = reshape(x, k, length(x)/k).';
xsym = bi2de(xsymce, 'left-msb');
%Separating HP & LP bits
HP_tx = horzcat(xsymce(:,1), xsymce(:,2));
LP_tx = horzcat(xsymce(:,3), xsymce(:,4), xsymce(:,5), xsymce(:,6));
%Modulation
ytxs = genqammod(xsym, constellation_ilow);
%Applying channel noise AWGN
EbNo=16;
EbNo_db=10*log10(EbNo);
yrxs = awgn(ytxs, EbNo_db, 'measured');
%Demodulation
zsym = genqamdemod(yrxs, constellation_ilow);
% convert integers to bits.
z = de2bi(zsym, 'left-msb');

HP_rx = horzcat(z(:,1), z(:,2));
LP_rx = horzcat(z(:,3), z(:,4), z(:,5), z(:,6));

[number_of_errors_HP, bit_error_rate_HP] = biterr(HP_tx, HP_rx)

[number_of_errors_LP, bit_error_rate_LP] = biterr(LP_tx, LP_rx)
```

Figure B.9: Matlab Code for BER vs SNR for SNR = 22 dB

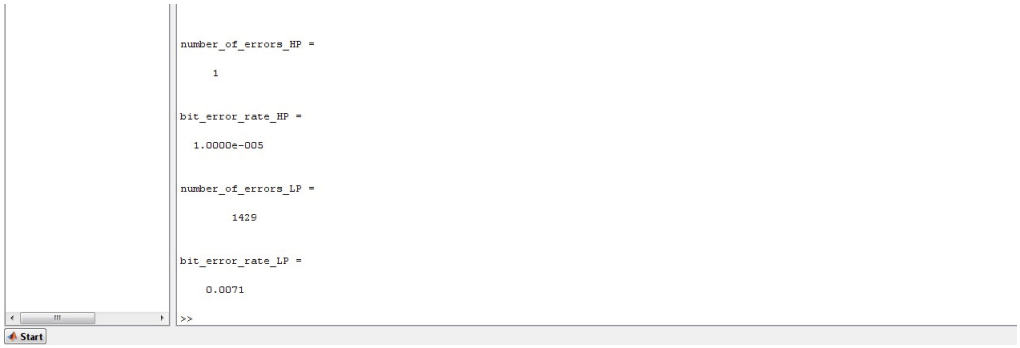

```
number_of_errors_HP =

     1


bit_error_rate_HP =

  1.0000e-005


number_of_errors_LP =

        1429


bit_error_rate_LP =

    0.0071

>>
```

Figure B.10: Simulation Results for BER vs SNR for SNR = 22 dB

Bibliography

[1] V. DeBrunner, L. DeBrunner, L. Wang, and S. Radhakrishnan, "Error control and concealment for image transmission," *IEEE Communications Surveys and Tutorial*, vol. 3, pp. 2–9, 2000.

[2] S. S. Hemami, "Robust image communication over wireless channels," *IEEE Commun. Mag.*, vol. 39, pp. 120–124, Nov. 2001.

[3] Y. Wang, J. Ostermann, and Y.-Q. Zhang, *Video Processing and Communications*. Prentice Hall, 2001.

[4] K. Rao, Z. Bojkovic, and D. Milovanovic, *Multimedia Communication Systems - Techniques, Standards, and Networks*. Prentice Hall PTR, 2002.

[5] F. Halsall, *Multimedia Communications - Applications, Networks and Standards*. Addison-Wesley, 2001.

[6] Kannan Ramchandran and Martin Vetterli, "Multiresolution joint source-channel coding for wireless channels," 1998.

[7] H. Datta and J. Ilow, "UEP framework in multiresolution modulation for robust image broadcasting," *IEEE 22nd Int. Symp. on Personal Indoor and Mobile Radio Communications (PIMRC-2011)*, pp. 551–555, Sept. 2011.

[8] K. Ramchandran, A. Ortega, K.M. Uz and M. Vetterli, "Multiresolution broadcast for digital HDTV using joint source/channel coding," *IEEE J. Select. Areas Commun.*, vol. 11, no. 1, pp. 6 –23, Jan. 1993.

[9] P. Vitthaladevuni and M.-S. Alouini, "BER computation of generalized QAM constellations," *IEEE Global Telecommunications Conference, 2001. GLOBECOM'01*, vol. 1, pp. 632 –636 vol.1, 2001.

[10] ——, "A recursive algorithm for the exact BER computation of generalized hierarchical QAM constellations," *IEEE Trans. Inform. Theory*, vol. 49, no. 1, pp. 297 – 307, Jan. 2003.

[11] M. van der Schaar and P. A. Chou, *Multimedia over IP and Wireless Networks: Compression, Networking, and Systems*. Orlando, FL, USA: Academic Press, Inc., 2007.

[12] C. Ong, J. Song, C. Pan, and Y. Li, "Technology and standards of digital television terrestrial multimedia broadcasting," *IEEE Commun. Mag.*, vol. 48, pp. 119–127, May 2010.

[13] K. S. Thyagarajan, *Still Image and Video Compression with MATLAB*. Wiley-IEEE Press, 2010.

[14] R. Hamzaoui, V. Stankovic, and Z. Xiong, "Optimized error protection of scalable image bit streams [advances in joint source-channel coding for images]," *IEEE Trans. Signal Processing*, vol. 22, no. 6, pp. 91 – 107, Nov. 2005.

[15] G. Strang, and T. Nguyen, *Wavelets and Filter Banks*. Wellesley-Cambridge Press, 1996.

[16] J. Shapiro, "Embedded image coding using zerotrees of wavelet coefficients," *IEEE Trans. Signal Processing*, vol. 41, no. 12, pp. 3445 –3462, Dec. 1993.

[17] A. Said and W. Pearlman, "A new, fast, and efficient image codec based on set partitioning in hierarchical trees," *IEEE Trans. Circuits and Sys. for Video Tech.*, vol. 6, no. 3, pp. 243 –250, Jun. 1996.

[18] D. S. Taubman and M. W. Marcellin, *JPEG2000 : image compression fundamentals, standards, and practice*. Kluwer Academic Publishers, Boston, 2002.

[19] D. Taubman, "High performance scalable image compression with EBCOT," *IEEE Trans. Image Process.*, vol. 9, no. 7, pp. 1158 –1170, Jul. 2000.

[20] P. T. P.M.K. Prasad and G. U. Madhuri, "Image Compression using Orthogonal Wavelets Viewed from Peak Signal to Noise Ratio and Computation Time," vol. 47, June 2012.

[21] B. B. Hubbard, *The World According to Wavelets*. A K Peters, 1996.

[22] L. Rowe, "Image Quality Computation," Sept. 2003. [Online]. Available: http://bmrc.berkeley.edu/courseware/cs294/fall97/assignment/psnr.html

[23] P. D. Seyed Bahram Zahir Azami and O. Rioul, "Joint Source-Channel Coding: Panorama of Methods," *IEEE Commun. Mag.*, November 1996.

[24] F. Hekland, "A review of joint source-channel coding," February 2004.

[25] B. Sklar, *Digital Communications: Fundamentals and Applications*, 2nd ed. Upper Saddle River, New Jersey: Prentice Hall, 2000.

[26] Sung-Joon Park, "Triangular Quadrature Amplitude Modulation," *IEEE Commun. Mag.*, vol. 11, pp. 2–9, 2007.

[27] S. Kozintsev and R. Ramchandran, "Robust Image Transmission Over Energy-Constrained Time-Varying Channels Using Multiresolution Joint SourceChannel Coding," *IEEE Commun. Mag.*, vol. 46, pp. 120–124, April 1998.

[28] J. G. Proakis, *Digital Communications*. McGraw Hill, 2000.

[29] K. Sayood, *Data Compression*. Academic Press, 2000.

[30] Y. Wang, J. Osterman and Y.Q. Zhang, *Video Processing and Communications*. Prentice Hall, 2001.